Funded by the
European Union

Compact

XLS-Report-2019-001
27 June 2019

XLS Deliverable D3.1

Preliminary assessments and evaluations of the optimum e-gun and injector solution for the CompactLight design

M. Ferrario[1)*], D. Alesini[*], F. Cardelli[*], G. Castorina[*], M. Croia[*], M. Diomede[*], A. Gallo[*], A. Giribono[*], J. Scifo[*], B. Spataro[*], C. Vaccarezza[*], A. Vannozzi[*], S. Di Mitri[†], R. Rochow[†], A. Latina[‡], M. D. Kelisani[‡], S. Doebert[‡], D. Angal-Kalinin[§], J. Clarke[§], E. Gazis[¶], A. Aksoy[‖], J. Luiten[**], A. Rajabi[**], X. Stragier[**], A. Faus-Golfe[††], Y. Han[††], D. Esperante[‡‡], M. Boronat[‡‡], C. Blanch[‡‡], J. Fuster[‡‡], B. Gimeno[‡‡]

On behalf of the CompactLight Partnership

Prepared on: 27.06.2019

[*] INFN, Italy, [†] ST, Italy, [‡] CERN, Switzerland, [§] STFC, UK, [¶] IASA, Greece, [‖] UA-IAT, Turkey, [**] TU/e, Netherlands, [††] CNRS, France, [‡‡] CSIC, Spain

[1] Corresponding author: massimo.ferrario@lnf.infn.it

Funded by the
European Union

Compact

This project is funded by the European Union's Horizon2020 research and innovation programme under Grant Agreement No. 777431. The contents of this report reflect only the view of the CompactLight Consortium. The European Commission is not responsible for any use that may be made of the information it contains.

Abstract

In this deliverable we report an overview of the possible injector options suitable to match the CompactLight X-band high brightness linac able to drive short wavelength FELs user facilities. Different schemes have been investigated including RF gun injectors at different operating frequency (S, C and X band) and a DC gun based design.

The electromagnetic and RF designs for all cases are reported and discussed, including a preliminary evaluation of the laser/cathode system requirements. Matchings with the downstream linac are also investigated with beam dynamics simulations.

State of the art S-band injectors look appropriate to achieve the required parameters at low repetition rate (100 Hz). On the other end a compact C-band (or X-band) RF gun design is expected to have even better performances at low repetition rates and moreover, due to the lower thermal load, could allow higher repetition rates operation, up to 1 kHz, with acceptable performances degradation. DC guns are also very promising solutions for kHz range operation.

Contents

1 Introduction

The optimization of the FEL parameters is quite a complicated task [1] but the main requirement for the electron beam in order to achieve short wavelength radiation in a reasonable undulator length (30-100 m) is clear: high transverse brightness $B_\perp$ to reduce the FEL gain length L_g according to the scaling: $L_g \propto B_\perp^{-1/3}$.

Transverse beam brightness is defined hereafter with the approximated expression: $B_\perp \approx \frac{2I}{\varepsilon_{n,x}\varepsilon_{n,y}}$, where I is the bunch peak current and $\varepsilon_{n,x,y}$ are the bunch transverse normalized emittances. The expected transverse brightness for electron beams driving short wavelength SASE FEL facilities is of the order of $10^{15} - 10^{16} A/m^2$. High brightness beam essentially means high bunch charge density (with peak currents of some kA) and low emittance ($\sim 1\mu m$). The difficulties to achieve such a high quality beam are partially mitigated by the fact that the FEL resonance condition implies that electrons slip back in phase with respect to photons by one radiation wavelength λ_r per undulator period λ_u. Hence radiation amplification occurs on the scale length of the slippage length $L_s = N_u \lambda_u$, where N_u is the number of undulator periods, typically much shorter than the bunch length, so that mainly bunch slice parameters are important for the FEL process. Wake fields effects in accelerating sections and in magnetic bunch compressors contribute to emittance degradation, hence the injector design and its operation is the leading edge for high quality beam production and for the success of the future light sources. RF and DC guns, photo-cathode materials, laser pulse shaping and sub-ps synchronization systems are evolving towards a mature technology to produce high quality and stable beams thus enabling the successful operation of short wavelength FEL user facilities [2

In a photoinjector the emitted electrons are rapidly accelerated to relativistic energies, thus partially mitigating the emittance growth due to space charge effects that is the dominant source of emittance degradation in a high brightness injector. One of the key feature that make RF photoinjectors so attractive is that the emittance growth is reduced when operated at high peak field as the one achievable in the RF gun: up to 120-140 MV/m in a S-band gun. In addition, the technique termed 'emittance compensation' [3] necessary to minimize the final injector emittance has been experimentally verified in many laboratories and theoretically well understood [4]. The optimal choice of the injector parameters and operating frequency is still subject of extensive investigations. From simple theoretical considerations [5], assuming approximately that the peak fields scales like the inverse of the RF wavelength, it follows that the injector peak brightness scales with RF wavelength and bunch charge as: $B_\perp \propto \lambda_{RF}^{-4/3} Q^{-2/3}$ showing that operation at low charge and high frequency is preferred. Operation at higher frequency and short RF pulses allow in principle higher peak field in the RF gun as it is desirable to damp space charge forces. The choice of the bunch charge is subtler. High charge (up to 1 nC) is preferred when a large number of photons are needed by the FEL users, on the other hand ultra-low charge per bunch (down to 1 pC) allows ultra-short FEL radiation pulses and FEL operation in the single spike regime [6]. On the other hand, DC guns equipped with thermionic cathodes have other advantages [7]. They can operate at higher repetition rate, ultimately CW operation, and are relatively simpler systems without the need of a laser to drive the photocathode. Thermionic cathodes have longer lifetime with respect to photocathodes and require limited maintenance, in addition the bunch charge distribution shows smooth electron population.

In the next sections we report an overview of the possible injector options suitable to match the CompactLight X-band high brightness linac able to drive short wavelength FELs user facilities. Different schemes have been investigated including RF gun injectors at different operating frequency (S, C and X band) and a DC gun based design aiming to achieve the target parameters at the injector exit listed in Table 1:

Table 1: Expected bunch parameters at the injector exit

Parameters	Units	After VB and / or BC1
Charge (Q)	pC	75
Beam energy	MeV	300
rms bunch length (σ_t)	fs	350
Peak current ($Q/\sqrt{12}\sigma_t$)	A	60
rms Energy spread	%	0.5
Projected rms norm. emittance	μm	0.2
Repetition rate	Hz	100-1000

The electromagnetic and RF designs for all cases are reported and discussed together with a preliminary analysis of the laser/cathode system requirements. Matching with the following linac are also investigated with beam dynamics simulations.

2 S-Band RF gun injector

2.1 State of the art S-band RF gun

S-band RF guns are a consolidated technology with many working examples fitting the necessary conditions for XLS FEL injector with low repetition rate (100 Hz) as specified in Table 1 describing the target parameters of the injector.

The LCLS RF gun is the state of the art technology for XFEL injectors see Fig. 1. The required beam brightness for the LCLS has been demonstrated. The main e-beam parameters are generated by a Cu cathode are summarized in the Table 2:

Table 2: LCLS injector parameters

LCLS Parameters	Units	Hard X	Soft X
Charge (Q)	pC	250	250
Beam energy	GeV	13.6	3.5
rms bunch length (σ_t)	μm	7	20
rms Energy spread	%	0.04	0.07
Injector projected rms norm. emittance $\varepsilon_x/\varepsilon_y$	μm	0.4/0.6	0.4/0.6
Repetition rate	Hz	120	120

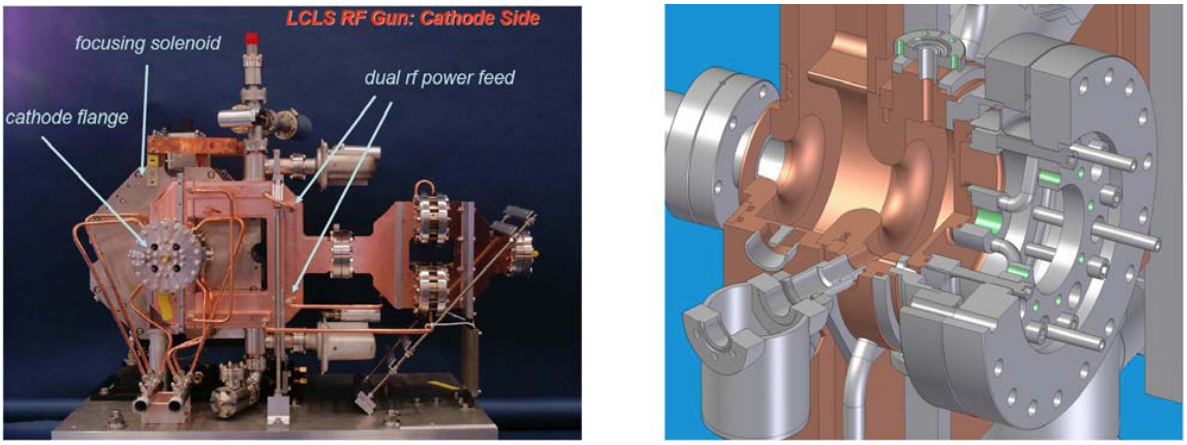

Figure 1: Left: LCLS RF gun viewed from cathode side, with dual RF feed, cathode flange and focusing solenoid. Right: LCLS RF gun in cut-away view showing the full and half cells with the cathode flange at right.

The LCLS RF gun is a modified version of the BNL/SLAC/UCLA symmetrized 1.6-cell RF photocathode gun [8] optimized to have the gun fields fully rotationally symmetric by incorporating a dual feed to eliminate dipole fields and a racetrack geometry to cancel quadrupole fields induced by the dual feed for the full cell into which the RF is coupled. In order to improve the reliability, the commonly used azimuth angle RF coupling has been replaced with much larger z-coupled ports running the full length of the cell. Furthermore, to reduce the pulse heating

and increase the gun lifetime a careful design of the lip radius was also made. The field emission from tuning slugs was eliminated by using deformation tuners. Finally, the shape of the iris between the two cells was modified to reduce (10 %) its surface fields below that of the copper cathode. The gun was first conditioned to 120 MV/m and 60 Hz. Conditioning at 120 Hz was limited to 107 MV/m due to excessive heating of the gun probes that has been redesigned to overcome this problem.

Another important innovation of the gun which improved its beam quality was to greatly increase the frequency separation of the 0-mode and π-mode until 15 MHz to reduce the excitation of the 0-mode, giving a pure π-mode in the gun.

The relative phasing between the gun and laser is established by running a 'Schottky scan', which varies the laser phase while measuring the accelerated bunch charge after the gun, giving minimum energy spread and minimal RF emittance growth. The transverse emittance is minimized by optimizing the main solenoid strength and by adding two small quadrupole coils incorporated into the gun-solenoid magnet. These coils were included to cancel a small quadrupole field error measured at the ends of the gun solenoid. One of these coils is wound to produce a 'normal' quadrupole and a second is wound as a 'skew' quadrupole. In addition to these quadrupole coils, a gun-solenoid bucking coil is included to cancel a small, measured longitudinal field on the cathode. A complete description of the design and commissioning could be found [9-13].

In recent times the S-band RF gun effort has been focused to reduce the realization cost of and to increase the repetition rate. In the following we will present the advances in these two aspects:

2.2 Reducing the cost and risk of the fabrication techniques

A crucial aspect after the RF design optimization phase is the optimization of the assembly process. This process implies in most of the cases a delicate and complicated brazing process. Recently novel fabrication techniques, avoiding brazing that strongly reduces the cost, the realization time and the risk of failure has been developed for short cell RF guns [14-16]. The technique is also being extended to longer Accelerating Structures, if successful it would provide a simple and inexpensive method of making copper accelerator structures.

Between the different brazing-free techniques we will present the RF gun developed, constructed and tested by INFN-LNF for the Extreme Light Infrastructure-Nuclear Physics Gamma Beam System (ELI-NP GBS) using special rf-vacuum gaskets [14, 15]. This RF gun represents a good candidate for the XLS FEL photo injector, the main parameters are summarized in table 3:

The ELI-NP RF gun is a further step in the new methodology of fabrication of complex RF structures at high-gradient and high-repetition rate.

The RF and thermomechanical design has been based in the LCLS but improved in different aspects, in particular: ELI-NP RF gun has been designed and tested for the 100 Hz repetition frequency with long rf pulses 1.5 μs and high average dissipated power 1 kW to sustain the

Table 3: ELI-NP injector parameters

ELI-NP RF gun Parameters	Units	
Resonant frequency	GHz	2.856
Cathode peak field	MV/m	120
Quality factor		146000
RF pulse length	μs	1.5
Repetition rate	Hz	100
Frequency mode separation	MHz	41.5
Working temperature	$^{\circ}$C	30
Charge per bunch	pC	250
Number of bunches		32
Beam emittance	mm mrad	<0.5
Cathode material		Cu

multi-bunch operation, and, to this purpose, the design of the cathode has been changed with an integrated cooling system; the maximum reached peak cathode field has been increased and successfully tested up to 120 MV/m; an improved technique to detect breakdown phenomena based on a fast digitiser and RF pulse shape masks has also been implemented; a thermomechanical design for the operation at 1 kW average dissipated power has been done. Fig. 2 shows de detail of the cooling system integrates six cooling channels with different diameters.

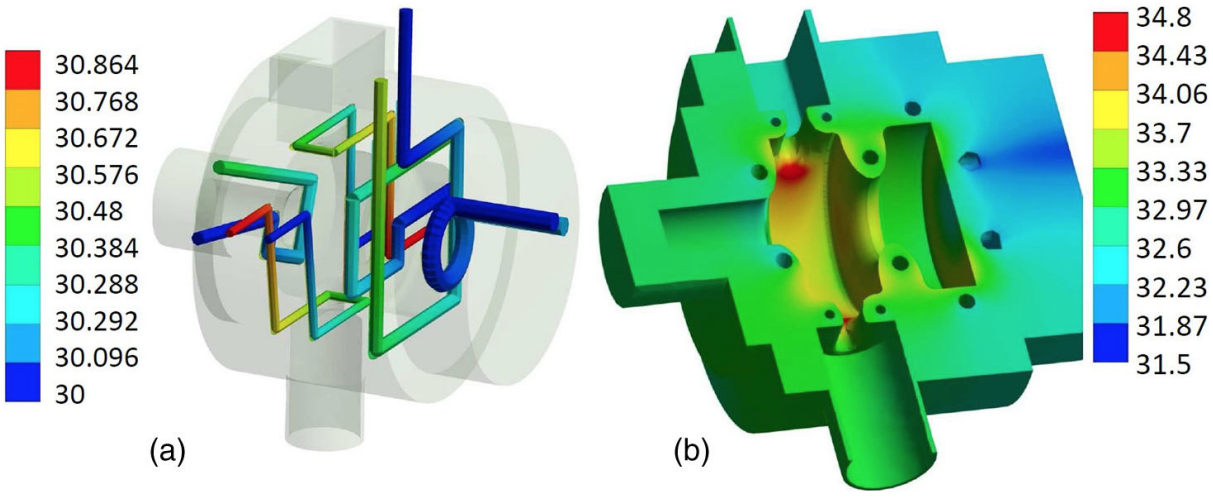

Figure 2: ELI-NP RF gun temperature distributed regimes: (a) water temperature in cooling pipes (b) gun body temperature.

Concerning the fabrication, the body of the gun has been fabricated from a single piece of OFHC copper using diamond tools. The rounded coupler geometry and the overall gun body have been realized with a five-axis milling machine. The full cell has then been sealed by clamping the body with the pipe by means of the special copper vacuum-RF gasket following the methodology sketched in Fig. 3, that simultaneously guarantees the vacuum seal and the

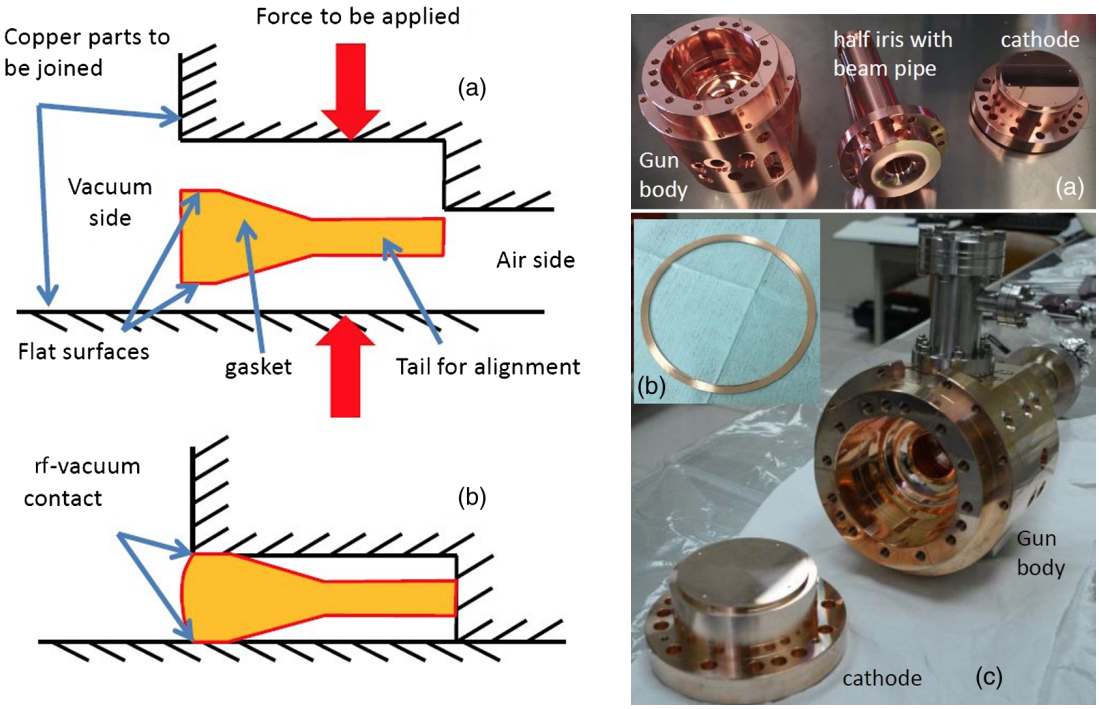

Figure 3: Left: Vacuum-RF gasket mechanism (a) uncompressed (b) compressed. Right: (a) Gun components before clamping (b) special gasket (c) gun assembly.

RF contact, avoiding sharp edges and gaps.

The gasket has not been annealed and has been compressed by a few hundred microns. This assures that it works in the elastic regime without damaging the surfaces of the gun body. All details are reported in [17].

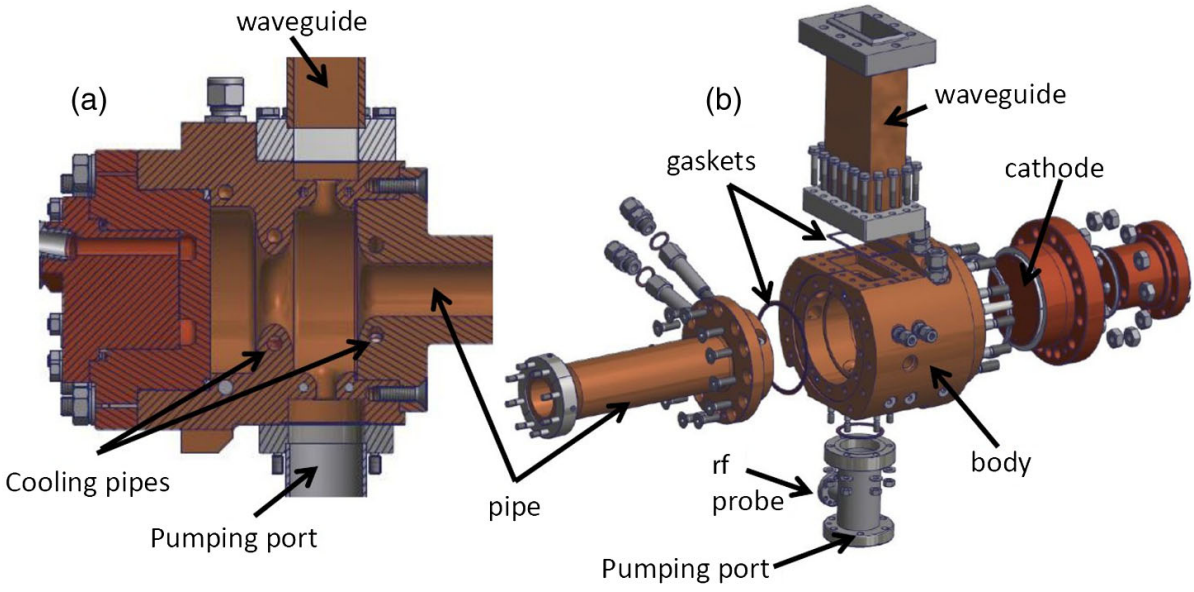

Figure 4: ELI-NP overall mechanical design.

The complete mechanical design is shown in Fig. 4.

The ELI-NP RF gun has been tested at low and high RF power [16] demonstrating the reliability and suitability of this new brazing-free technique for high gradient and high repetition RF guns and opens the possibility of implementing this methodology in longer RF multicell structures as illustrated in Fig. 5.

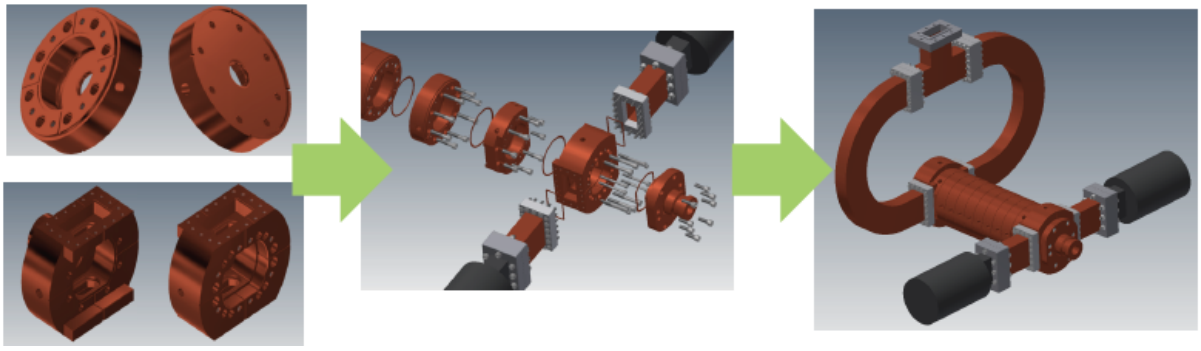

Figure 5: ELI-NP overall mechanical design.

2.3 Increasing the repetition rate

Another important issue in the research of the S-band RF gun is the increase of the repetition rate. In that sense a High-Repetition Rate (HRRG) RF gun is being developed to meet the high-brightness required for the proposed CLARA FEL test facility at Daresbury Laboratory [18]. The system comprises a 400 Hz RF Gun providing high brightness electron bunches with a charge of up to 250 pC. The main parameters are summarized in Table 4:

Table 4: CLARA injector parameters

CLARA FEL RF gun Parameters	Units	100 Hz	400 Hz
Resonant frequency	GHz	2.998	2.998
Cathode peak field	MV/m	120	100 / 80
Quality factor		13350 (Mo) / 14230(Cu)	
Repetition rate	Hz	100	400
Average RF power	kW	2.45	6.8 / 4.35
Working temperature	$^{\circ}$C	48	
Temperature stability	$^{\circ}$C	0.91	0.1
Charge per bunch	pC	20-250	250
Beam emittance	mm mrad	0.5	
Cathode material		Metal/Cs_2Te	

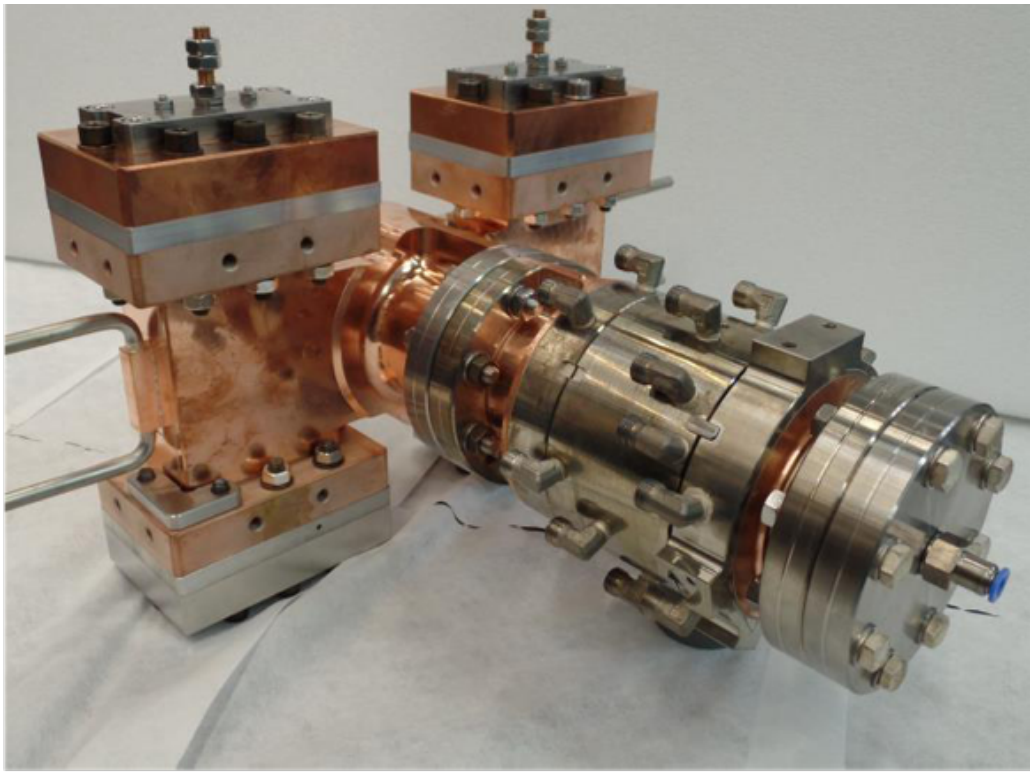

Figure 6: HRRG CLARA RF gun after manufacturing by RI GmbH.

The final design is based on a 1.5 cell normal conducting S-band RF cavity [19]. It has a dual feed RF input coupler with phase adjustment of each feed which has been shown in simulations to suppress any dipole component in the coaxial coupler line. The manufactured RF gun is shown in Fig. 6. The practical limit in the described design has been set as 120 MV/m which is current state of the art for similar designs. For operation with a repetition rate of 400 Hz, a maximum surface field of 100 MV/m has been specified.

These requirements imply power handling capabilities of 6.8 kW on the gun cavity. A special effort has been made in the design of the cooling system. The thermal stabilization of the gun cavity is achieved via 9 individual cooling channels as shown in Fig. 7, the flow through which can be controlled remotely and used to optimize frequency and field flatness under various operating conditions. The cell radii are expected to increase by 5.6 μm due to the average steady state RF load of 6.8 kW at 400 Hz and 100 MV/m. This gives a detuning of the resonance frequency of -0.427 MHz which will be compensated for in the water temperature stabilization system. All details about the thermos stabilization system could be found in [20, 21].

The photocathodes are interchangeable $metal/Cs_2Te$ and the plug design and transport system are compatibles with the ones used DESY/LBNL/FNAL.

The beam focusing and emittance compensation are provided by a pair of coaxial water-cooled solenoids mounted magnetized in opposite directions such that the fields they generate at the location of the cathode cancel each other out. The magnetic system is operated at variable solenoid currents and at variable separation between the solenoids to produce optimum parameters of the emitted beam.

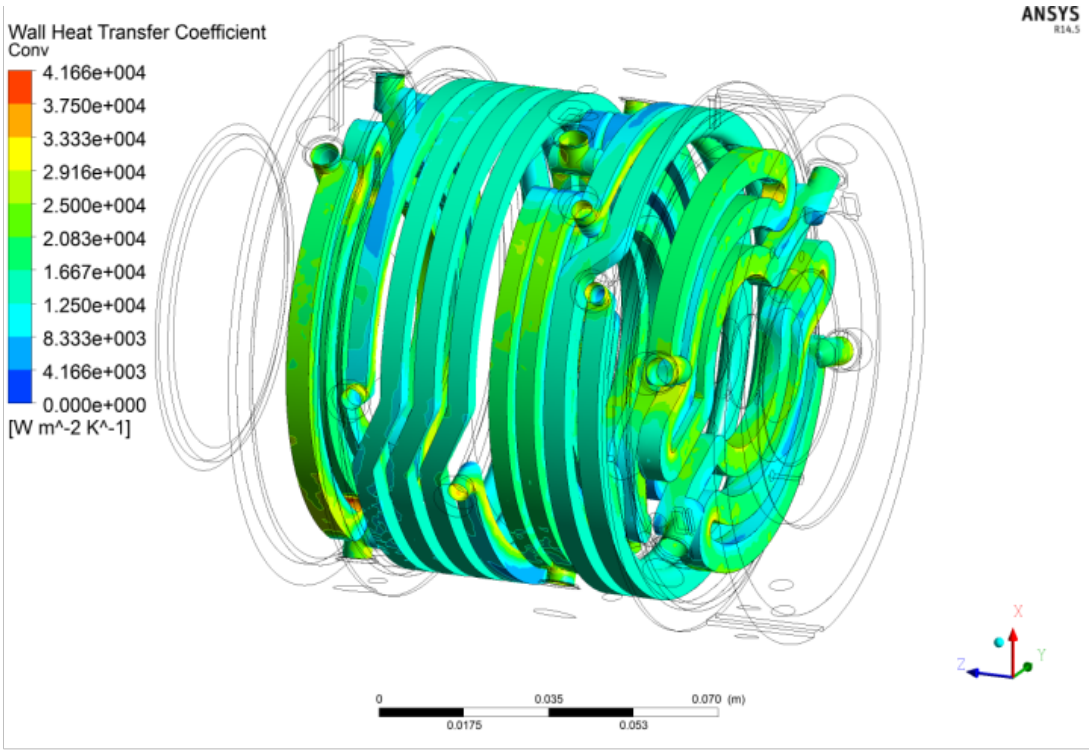

Figure 7: Wall convective heat transfer modelisation in HRRG CLAR RF gun.

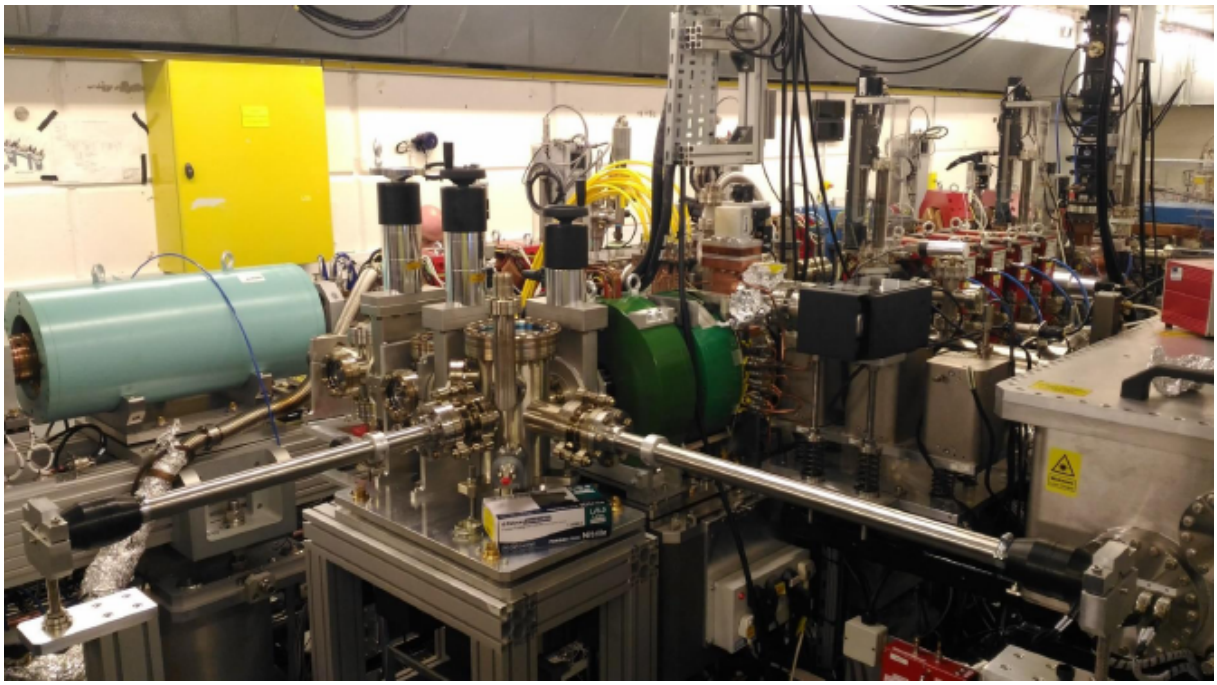

Figure 8: HRRG CLARA RF gun at commissioning in VELA-CLARA facility at Daresbury.

The low-power tests have been successfully made and the RF gun is currently under high-power commissioning at VELA-CLARA facility at Daresbury as shown in Fig. 8.

2.4 S-band gun with x-band booster

A very compact and simple alternative injector for CompactLight could be a hybrid consisting of a regular 1.6-cell S-band RF-GUN with a peak field of 120 MV/m followed directly by an x-band module used for velocity bunching and acceleration. The x-band hardware used is the baseline CompactLight structure at 65 MV/m surrounded by solenoids for the injector. The injector would have a length of about 9 m to reach 300 MeV. The usage of the well proven S-band gun reduces the risk and allows for good pumping and laser coupling. The ASTRA simulation used uniform laser distributions with a spot size of 0.3 mm and a laser pulse length of 4 ps. The bunch charge was set to 75 pC and the thermal emittance amounts to 0.11 μm. It is of course possible to simply accelerate and obtain an excellent emittance of the order of the thermal emittance.

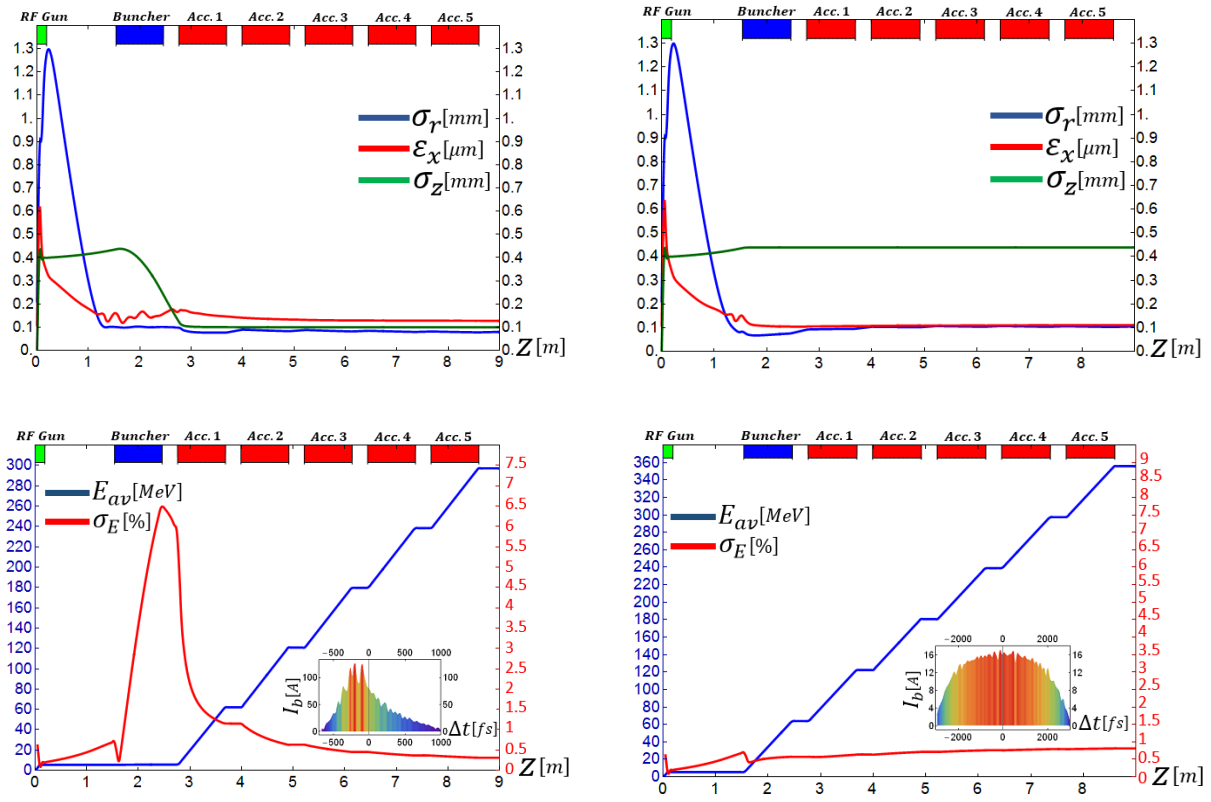

Figure 9: Performance plots of an S/X-band hybrid injector using a 75 pC bunch charge. Left plots with velocity bunching to 350 fs and right plots without velocity bunching. In both case the emittance is below 0.2 μm. An almost regular x-band module can be used directly after the S-band RF-GUN.

Due to the x-band acceleration however the energy spread rises to 0.8 % at 350 MeV. Using high frequency acceleration makes more sense in combination with velocity bunching. In the second example, (see Fig. 9) a moderate compression was applied using the first x-band structure to arrive at a final bunch length of 330 fs. The energy spread is 0.3 % at 300 MeV and the emittance 0.13 μm. This beam has been tracked through the linac and can be successfully compressed further to reach peak current of a few kA without using a lineariser. It is possible to apply more velocity bunching to arrive at a bunch length, which would allow omitting BC1. The emittance rises in this case to just below 0.2 μm. It remains to be studied how such a

beam performs in the following linac.

In conclusion S-band RF gun is a mature technology solution for future very high-brightness FEL applications. An important effort has been made in the recent years to simplify the fabrication process with new free-brazing techniques and to improve the repetition rate. An important R&D effort has to be made to get higher repetition rates as 1 kHz, not only from the point of view of the thermal stabilization but also from the high-power point of view to make commercially available klystrons.

3 C-Band RF gun injector

The schematic layout of the full C-band injector we are proposing is given in Fig. 10. The C-band gun is followed by two C-band TW structures that we have scaled, to the first order, by those developed for the SwissFeL [22] and that can operate with a single klystron and a pulse compressor at the level of 40 MV/m. The solenoids after the gun and around the TW structures allow to keep under control the beam emittance increase also in case of longitudinal compression by velocity bunching [23].

The correct scaling laws for the cathode field [6], indicate that, in order to gain in term of emittance and brightness one has to scale $E_{cath} \propto \lambda_{RF}^{-1}$. This drives to the conclusion that, in C-band, if we want to scale the working points of the S band guns we have to reach a cathode peak field of 240 MV/m. The design of the gun is focused to achieve such a high gradient keeping under control all known quantities that drive the breakdown phenomena.

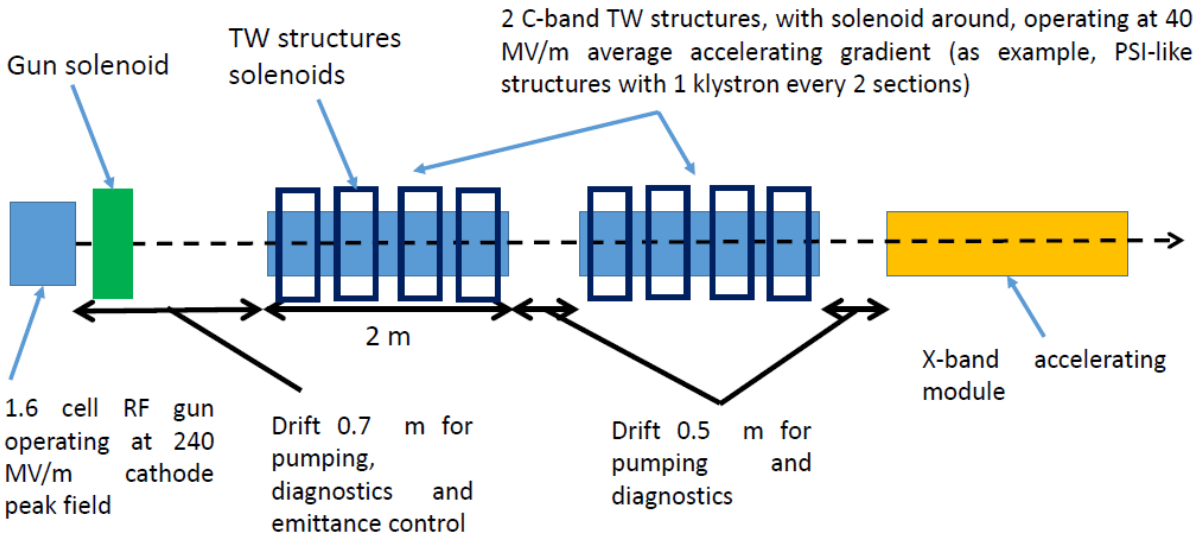

Figure 10: Schematic layout of the C-band injector.

In the design of the gun we have considered that, according to the high gradient test performed on X-band structures, there are three main quantities that allow to control and predict, in principle, the final BDR in a radiofrequency (RF) structure. Such a quantities are: the peak E field (E_{cath}), the modified Poynting vector (S_c) [24], the RF pulse length (t_p) and Pulsed Heating (ΔT) [25]. In particular, if $E_{cath} \leq 240 MV/m$, $t_p \leq 180$ ns, $S_c \leq 6 W/\mu m^2$ and $DeltaT \leq 40$ °C, the expected BDR is less than $2x10^{-6}$ bpp [26]. The two quantities S_c and ΔT can be kept below these values with a proper design of the cells and couplers, while short RF pulses can be used if we increase the input peak power and if we properly choose of the coupling coefficient (β). The optimized 2D profile of the gun with main dimensions are given in Fig. 11 while its main parameters are reported in Table 5.

The required input and reflected powers as a function of β and for different pulse lengths are given in Fig. 12. We have finally fixed β = 3, an input power of 40 MW and a pulse length of 180 ns.

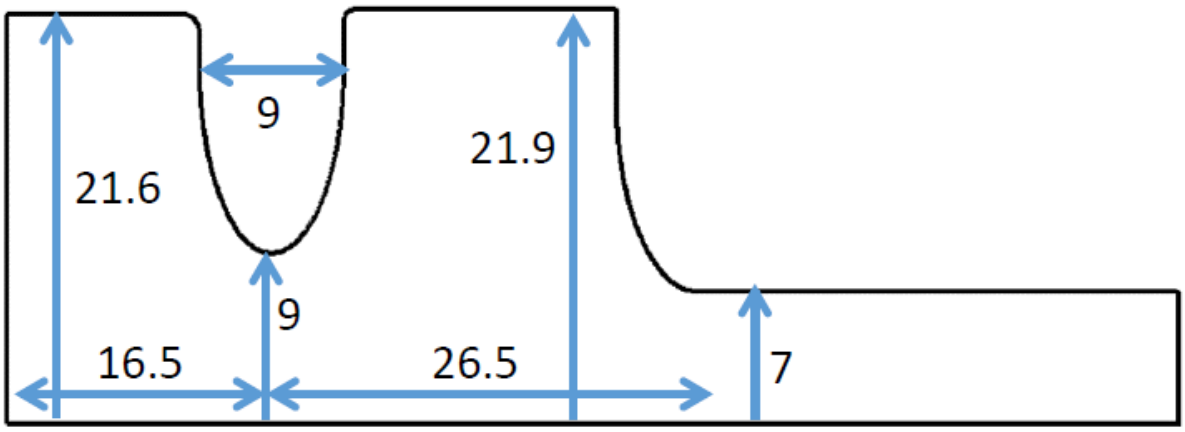

Figure 11: 2D gun profile with main dimensions (in mm).

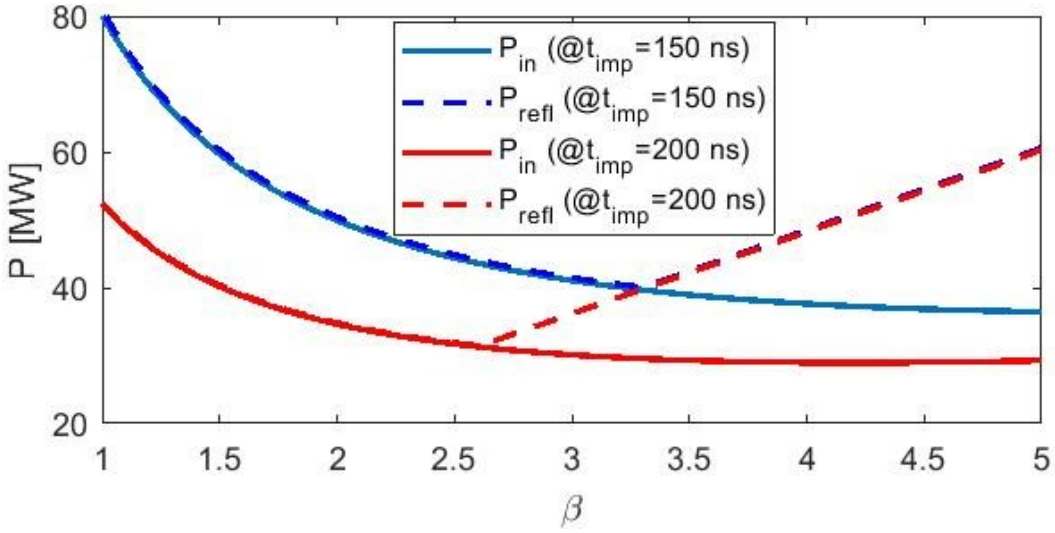

Figure 12: Required input and reflected powers as a function of β and for different pulse lengths.

Standard couplers on the full cell, even if strongly rounded [27,28] cannot be used because of the high magnetic field and, as a consequence, high pulsed heating on the coupling holes. For this reason, two different solutions have been explored and are schematically represented in Fig. 13. The first type of coupler is a mode launcher-type coupler [29] while the second one is a new coupler we have proposed that operate on the TM_{020} mode on the full cell. This allow to couple the field in the waveguide, electrically, strongly reducing the pulsed heating. There are advantages and disadvantages in the two solutions. In particular, the second type of coupler allows to use a solenoid immediately after the gun simply scaled from S-band guns. On the contrary the mode launcher one needs the development of a new solenoid with large bore and bucking coils to cancel the magnetic field on the cathode. The first type of coupler shows also a larger ratio $E_cath/\sqrt{P_{diss}}$ and is mechanically more simple, it also allows a better and uniform cooling of the accelerating cells.

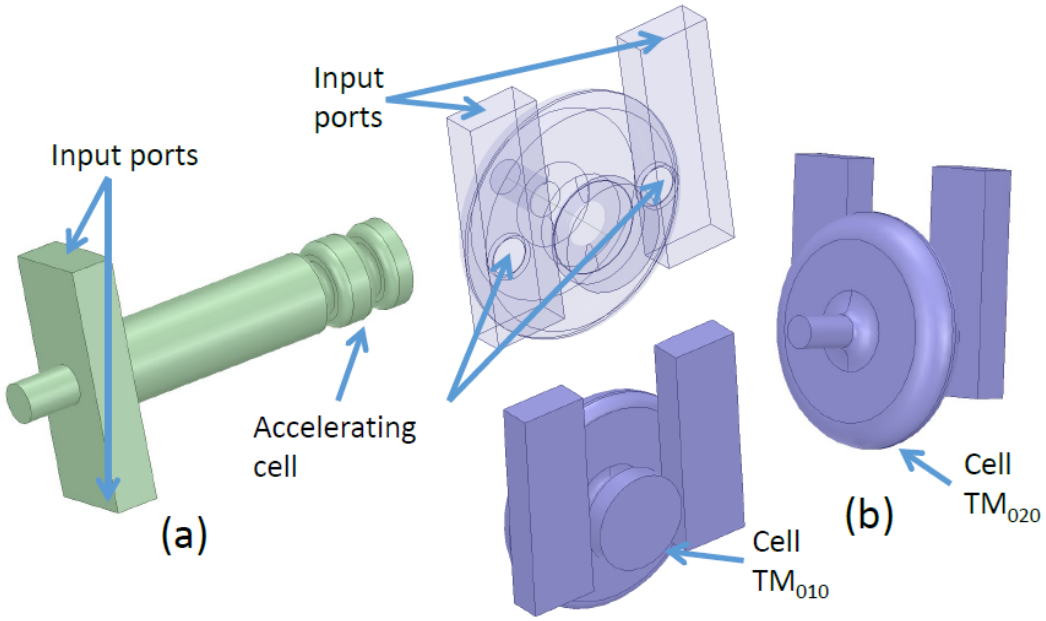

Figure 13: Proposed input couplers: (a) mode launcher type; (b) new coupler with TM020 cell.

Table 5: Main parameters of the C-band gun (the values in parenthesis are referred to the TM_{020}-type coupler).

Parameters	Value
Resonant frequency [GHz]	5.712
$E_{cath}/\sqrt{P_{diss}}$ [MV/(mMW$^{0.5}$)]	65 (55)
RF input power [MW]	40 (70)
Cathode peak field [MV/m]	120
Repetition rate [Hz]	100
Quality factor	11000 (14000)
Filling time [ns]	150
Coupling coefficient	3
RF pulse length [ns]	180
Mode separation 0 -π [MHz]	
Pulsed heating [$^{\circ}$C]	<40
Average did. Power[W]	200

Concerning the feeding system, two possible solutions are schematically represented in Fig. 14. Commercial circulators, able to handle 50 MW input/reflected power, already exist in C-band [30] and also pulse compressors that can manage up to 300 MW output power have been developed in C-band [31]. The second proposed scheme is more flexible and allows, in principle, to explore even shorter pulses.

The working point of the injector has been scaled from the well-known S-band injectors. To this purpose the longitudinal lengths of the devices (cavities and magnets) have been scaled by a factor two and the fields (electric and magnetic) have been doubled with respect to the S-band case. We used the simulation code GPT [32] with 20k particles for fast parameters

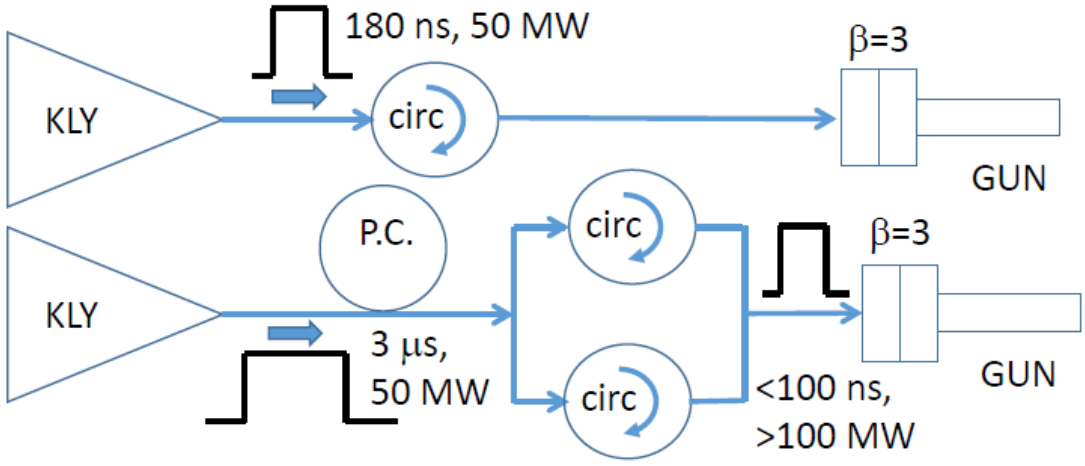

Figure 14: Possible feeding systems.

scans while the final simulations have been done using 250k particles.

The laser parameters have been scaled using the formula reported in [6] to have the same bunch charge density of the LCLS and SPARC_LAB cases [33-36] adopting the same emittance compensation technique. The intrinsic emittance [37,38] has been calculated, for the copper cathode, considering the ideal case of a flat cathode (i.e. field enhancement factor $\beta_{rf} \approx 1$) giving $\varepsilon_{int} \approx 0.8 \mu m/mm$.

We have analysed the two cases of on crest acceleration and longitudinal compression using the velocity bunching technique [39], to match the XLS requirements. In this second case the solenoids around the two C-band structures have been tuned to keep under control the spot size and the emittance. The final normalized emittance on crest and in the compression case are the same and equal to $\varepsilon_{n,rms} \approx 0.15 \mu m$.

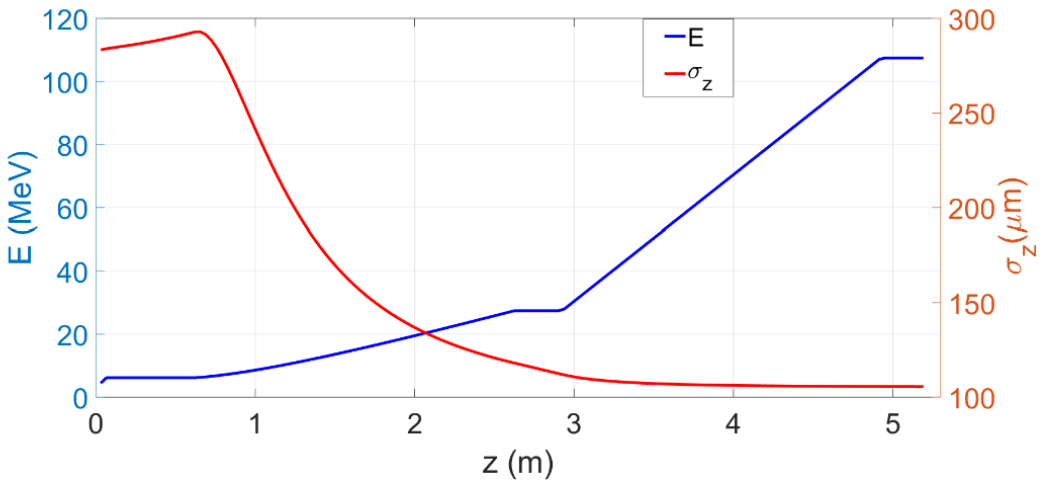

Figure 15: Evolution of the beam energy and bunch length along the C-band injector.

Figs. 15 and 16 show the evolution of the main beam parameters along the injector itself while Table 6 summarize the beam parameters at the end of injector in the two cases. One of the

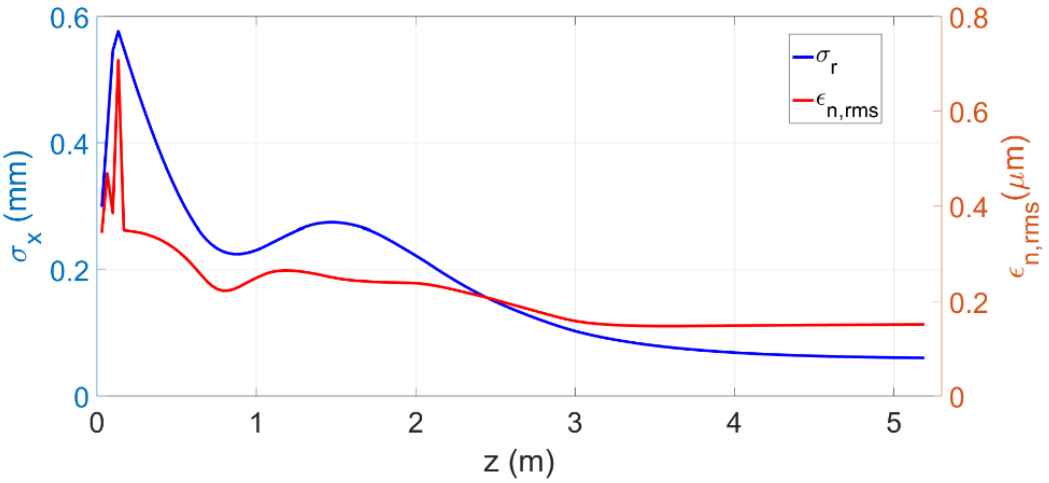

Figure 16: Evolution of the beam envelope and emittance along the C-band injector.

main advantages of this high gradient gun is to quickly freeze the emittance after the cathode, dumping in a shorter distance, the space charge forces. This is important to reduce the non-linear space charge contribution to the emittance that cannot be reduced using the emittance compensation scheme. Moreover, the beam at the exit of the injector can be directly injected into X-band modules.

Table 6: Main beam and laser parameters at the end of injector in two cases: with and w/o bunch compression.

Parameter	w/o BC	with BC
Laser spot size [μm]	294 uniform	
Laser rms length [ps]	13.4	
Rise time laser pulse [fs]	600	
Bunch charge [pC]	75	
Beam emittance [mm mrad]	0.15	
Bunch length [μm]	295	105
Beam Energy [MeV]	170	107
Peak current [A]	22	60
Beam energy spread [%]	0.6	1.4

4 X-Band RF gun injector

The RF photoinjector design presented here is based on a 5.6 cells standing wave structure operating with the π-TM_{010} mode of the cylindrical cavity. The way to couple the RF power from the generator to the RF photo-gun is by means of a coaxial waveguide coupler, which preserves the circular symmetry of the entire device. First, the RF design of the structure is optimized to fulfill the desired specifications (RF electric field profile in cells to ensure proper electron acceleration, operating frequency, etc.). This task was performed using the software SUPERFISH [40]. After this, an exhaustive analysis of the RF electromagnetic performance of the RF photoinjector was carried out, taking into consideration the RF pulse heating, the RF breakdown risk due to the presence of high intensity RF electromagnetic fields, and the multipactor discharge risk at the coaxial coupler.

4.1 RF gun design

The photoinjector scheme is shown in Fig. 17 and is similar to other RF guns developed for X-band operation [41.42]. It consists of six accelerating cavities each of them with length $\lambda/2$ (being $l\lambda$ the wavelength of the RF electromagnetic wave in vacuum), but the first cell, which has a length of 0.6 times the others. The cells are coupled by means of elliptical irises, which have been found to be better than circular irises in order to reduce the RF electric field at the gun surfaces [42]. The RF gun is connected to the RF generator external circuit by means of a coaxial coupler. Due to the choice of this coupling scheme, the entire RF gun structures preserves the circular symmetry, allowing to use the SUPERFISH software. SUPERISH is a 2D code suitable for solving RF electromagnetic problems with circular symmetry, and it presents the advantage of being much faster than 3D commercial software such as Ansys HFSS or CST Microwave Studio.

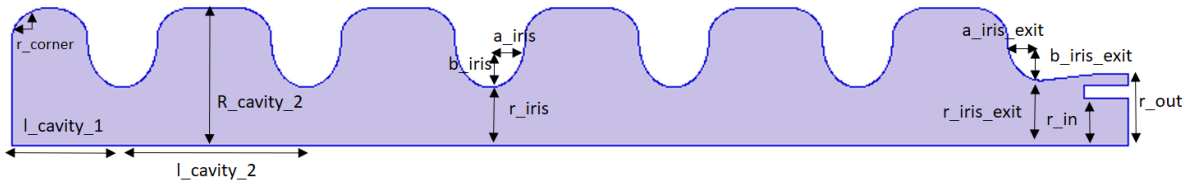

Figure 17: Scheme of a 5.6 cell RF gun with a coaxial coupler.

The design of the RF gun has been carried out in two steps. In the first one, the RF gun is divided in three different parts: the central cells, the first (cathode) cell, and the last cell with the coaxial coupler. For each of these pieces of the gun is performed a separate design optimization in order to reach the set of goal design values. With regard to these design objectives, each piece has to be tuned to the desired operating RF frequency. Moreover, the shape of the cells is essayed trying to minimize the RF electric field at surfaces with regard to the corresponding cathode value, in order to reduce the RF breakdown risk. At the same time, the gun geometry has to try to maximize the separation between the operating π-mode and the nearest neighbor mode in order to avoid the residual excitation of such mode during the RF transient.

Table 7: Dimensions of the RF gun.

labeltab:dimensions

Parameter	Value (mm)
$R_{cavity1}$	10.97645
$R_{cavity2}$	11.02895
$R_{cavity3}$	11.03540
$R_{cavity4}$	11.03554
$R_{cavity5}$	11.03379
$R_{cavity6}$	11.01544
$l_{cavity1}$	7.499
$l_{cavity2\rightarrow6}$	12.498
r_iris	4.624
r_corner	2.460
a_iris	2.362
b_iris	3.627
$r_irisexit$	5.16815
r_out	5.800
r_in	3.800
$a_irisexit$	2.30821
$b_irisexit$	3.24009
deltar	1.0
z_ins	2.930

Finally, the output cell with the coupler has to match with the desired coupling factor β. In the second design step, the previous three tuned pieces of the gun are merged together to conform the 5.6 cell RF gun structure. The resulting device is optimized to achieve an equal value for the maximum modulus of the axial electric field in all the gun cavities, at the same time preserving the other objectives (resonant frequency and coupling factor).

For the current X-band RF gun design, the following goals have been set: resonant frequency of the π-mode, f = 11.994 GHz; coupling factor β = 1, and maximum modulus of the axial electric field in all cavities. The final design dimensions are summarized in the next Table 7.

For such gun dimensions, it is obtained a resonant frequency f = 11.993996 GHz, a coupling factor of β = 1.005, and a separation between the π-mode and the nearest neighbor mode of Δf = 27.1 MHz. Besides, the equality in maximum electric field modulus along the axis for each cavity is better than 99% as it can be observed in left of Fig. 18. With regard to the maximum RF electric field at gun surfaces is max(E_{sup}) = 0.988 MV/m for a cathode RF electric field of 1 MV/m (see right of Fig. 18), i.e., slightly lower than this, as required in the design specifications.

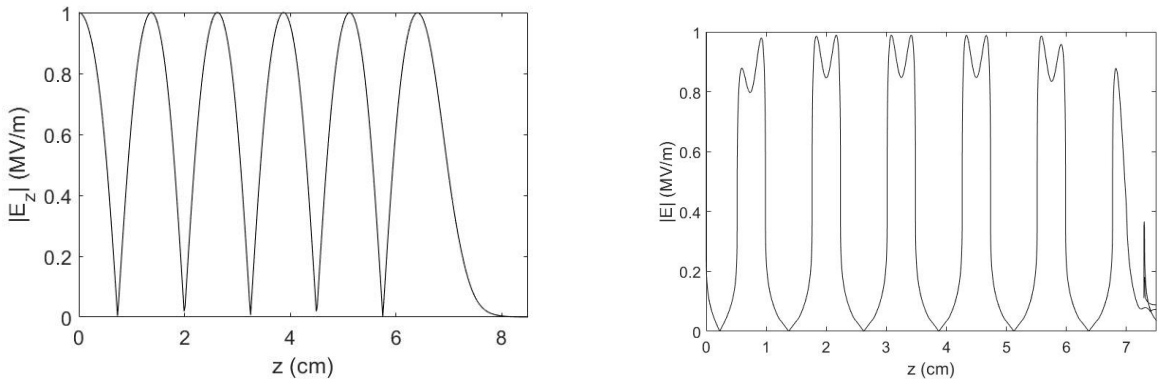

Figure 18: Left: modulus of the axial RF electric field along the gun axis. Right: modulus of the RF electric field at the gun surfaces along the gun.

In order to guarantee that the previous results are accurate enough, a convergence analysis was performed in SUPERFISH. To do this, different mesh space sizes were employed to sim-

ulate the RF electromagnetic fields and to obtain the main gun parameters. In Fig. 19 it is shown the results from this study for the RF axial electric field along the gun axis.

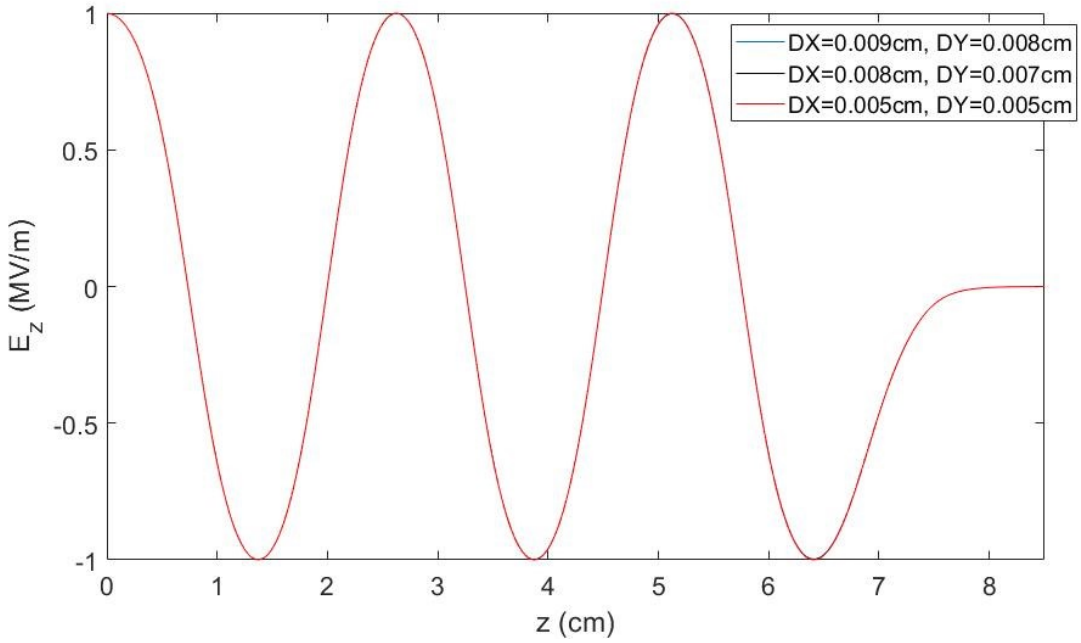

Figure 19: RF axial electric field along the gun axis for different values of the mesh spacing in SUPERFISH.

4.2 Multipactor analysis in the coaxial coupler

During the RF gun operation the coupler coaxial line will be exposed to high-power RF electromagnetic fields that may cause the appearance of multipactor discharges3. The multipactor effect is a resonant vacuum electron discharge that appears in components operating with RF high-intensity electromagnetic fields. When certain conditions are satisfied, the free electrons synchronize with the RF electric field, and impact against the metallic walls releasing secondary electrons. Thus, the increase of the electron population in the device leads to an electrical discharge that degrades the component performance and can physically damage the structure.

With the purpose of assessing the multipactor risk in the coaxial coupler, a set of multipactor numerical simulations were performed at different levels of RF power in order to obtain the multipactor susceptibility zones in which the discharge is expected to occur. The multipactor numerical simulations for the coaxial line were carried out with an in-house developed code based on the Monte Carlo method and it is based on the single effective electron model [43]. This technique is based on the 3-D tracking of a set of effective electrons governed by the electromagnetic field. The trajectory of the effective electron is found numerically solving its equation of motion by means of the Velocity-Verlet algorithm. Each effective electron describes a particular electronic population that evolves in time by colliding with the coaxial metallic walls of the waveguide. The secondary electron yield (SEY) function is computed after each impact as a function of the impact kinetic energy and impinging angle by means of the SEY model formulated in [44]. After that, the colliding electron is reemitted from the impact place with

random initial velocity given by a Maxwellian distribution with a mean average energy of a few electronvolts. The driving electromagnetic field experienced on each effective electron is the corresponding to the fundamental TEM mode of the coaxial guide at frequency that the RF gun operates.

According to the results of the numerical simulations there are two multipactor windows that span over the RF voltage amplitude ranges that are indicated in the Table 8.

Table 8: Multipactor susceptibility windows for the coupler

Multipactor window	P (MW)	V(kV)
1	0.035-0.56	0.891-3.565
2	1.20-3.10	5.219-8.388

At the RF power level that the gun is intended to operate (i.e., with a RF electric field value of 200 MV/m at cathode), the RF voltage in the coaxial line is 13.226 KV, which is above the second multipactor window, so no multipactor discharge is expected at this point. However, when the RF power is turned on, there is a transient behaviour for the RF electromagnetic field both in the coaxial line and in the RF gun cavity until the RF electromagnetic field amplitude reaches the stationary value in which is intended to operate.

Despite the multipactor risk is possible at the coupler during the transients, it does not represent a crucial problem since it can be suppressed by means of an external magnetic field. This fact has been theoretically and experimentally demonstrated for a coaxial line in [45], where also are outlined the following two conclusions. The first one is that the multipactor can always be suppressed provided that a strong enough magnetic field is applied along the coaxial axis. The second conclusion provides an empirical approximate rule that allows to estimate the minimum magnetic field value $B_{dc,min}$ required to suppress the discharge. For the RF gun operating frequency this approximation gives a value of 428.5 mT. In order to confirm such prediction, additional multipactor numerical simulations were performed taking into consideration the presence of the dc axial magnetic field. The results evidence that no multipactor discharge is expected when such external magnetic field is applied. Moreover, numerical simulations revealed that a dc magnetic field of 360 mT is enough to suppress the discharge in the coaxial. Accordingly, a solenoid with such magnetic field value (or higher) will be included in the RF gun design for multipactor mitigation in the coupler coaxial line as well as for emittance compensation purposes.

4.3 RF breakdown

RF breakdown is a phenomenon that appears in RF accelerating structures when high gradient surface electric fields (hundreds of MV/m) are present. In such conditions, an electric current is emitted from the walls of the device forming a plasma that increases suddenly the vacuum pressure level. Moreover, non-linearities that degrade the beam performance (emittance, acceleration, luminosity) emerge as a consequence of the interference between the emission current and both the RF input power and the resonant cavity. The risk of RF breakdown in a

component is assessed by means of the breakdown rate (BDR) which is defined as the expected number of breakdowns per pulse and meter length of the structure. According to ref. [24], the BDR can be calculated by obtaining the modified Poynting vector S_c along the device surfaces.

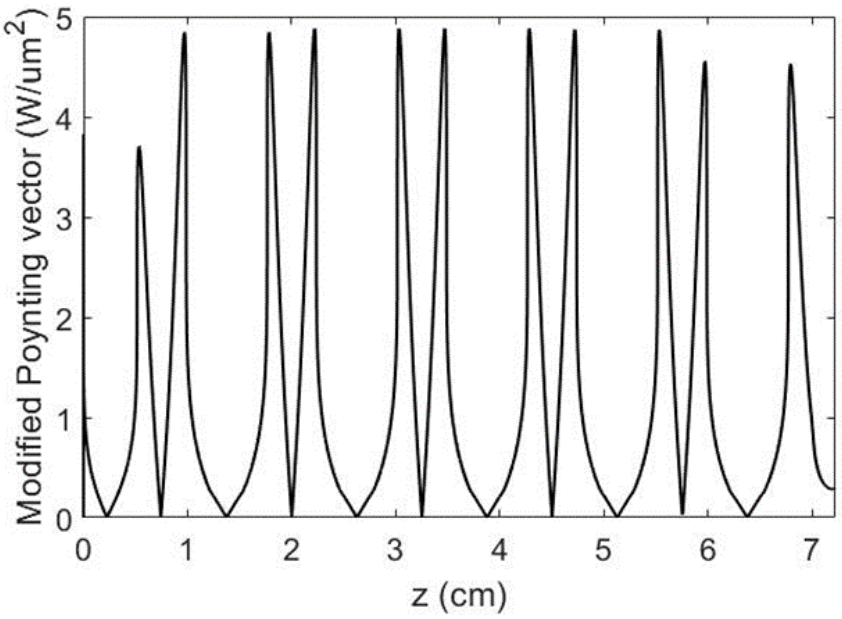

Figure 20: Modified Poynting vector at the RF gun surfaces.

In the Fig. 20 it is shown the results for the modified Poynting vector along the gun surfaces, assuming a 200 MV/m cathode field and g_c = 1/6, see [24]. The maximum value of S_c for the gun is 4.88 W/μm^2.

In Fig. 21 it is shown the maximum BDR in the RF gun as a function of the time that the RF signal is on, assuming a cathode field of 200 MV/m at the stationary state. Both the results provided by the time constant $S_{c,0}$ model [24] and time varying S_c(t) model are included for comparison. As expected, it is observed that when Ton » tF, the BDR given by Sc(t) approaches to the corresponding to $S_{c,0}$.

4.4 RF pulse heating

RF pulse heating is a phenomenon that appears due to Joule effect caused by the induced electric currents in the metallic walls of the accelerating structures operating under high-intensity RF electromagnetic fields, resulting in a temperature increase of the device surfaces. This temperature increase is harmful for the operating device and an excessive heating can even increase the risk of RF breakdown.

The RF magnetic field component parallel to the device surface $H_{\|}$ penetrates a certain depth into the metal, thus inducing an RF electric field that, due to the finite conductivity of the metal σ, deposits an amount of power P into the walls as heat.

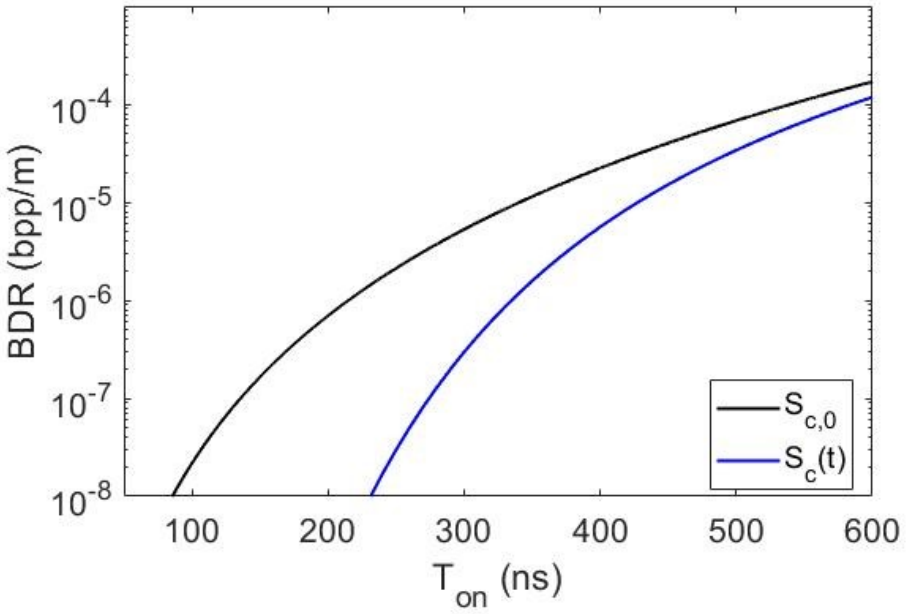

Figure 21: Maximum BDR in the RF gun (for a 200 MV/m cathode field at the stationary state) as a function of the time that the RF generator is on. For the RF gun tF = 112.5 ns.

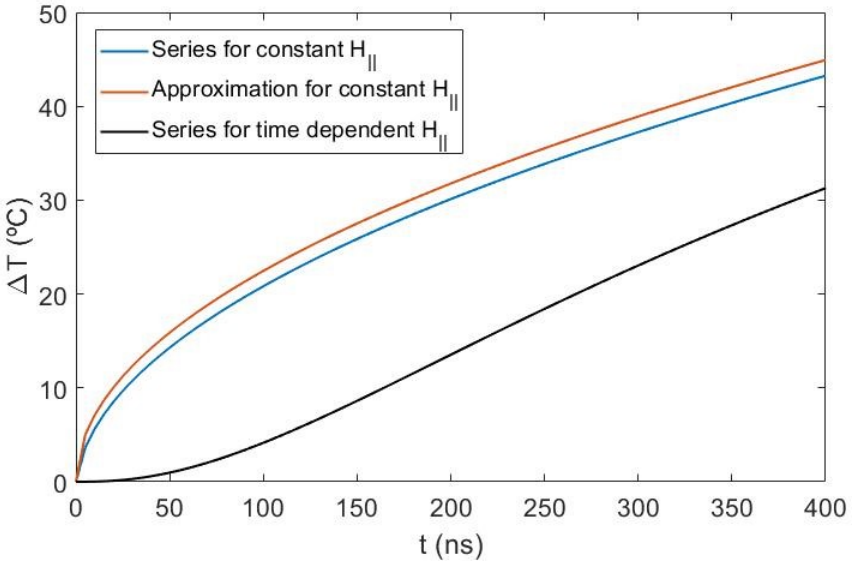

Figure 22: Maximum temperature increase in the gun surfaces (when operating with 200 MV/m cathode field) for as a function of time, for ton = 400 ns. Results for the H|| constant amplitude assumption are included for comparison.

The results obtained for the RF gun taking in to account the transient effects are shown in Fig. 22, evidencing the over-estimation of the RF pulse heating given by the constant H|| amplitude assumption solutions. According to our [46] accurate results, the maximum temperature increase in the RF gun is around 31°C for a generator pulse length of t_{on} = 400 ns. This warming value is below the maximum temperature increase recommended by the authors in the technical literature ([47] and [48,49]).

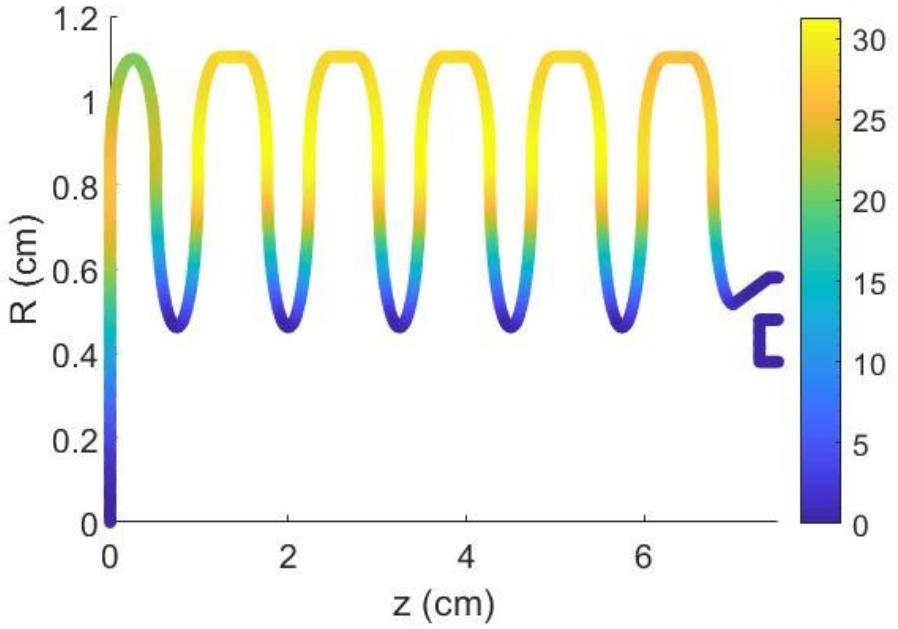

Figure 23: Temperature increase (according to eq. 5) in the gun surfaces when operating with 200 MV/m cathode field at a time t = 400 ns, for ton = 400 ns.

Finally, it is also interesting to depict the local temperature increase at the different surfaces of the RF gun, as it is shown in Fig. 23, to assess the critical regions of the gun where the warming becomes more noticeable.

4.5 Summary

In Table 9 the fundamental parameters that describe the RF performance are summarized.

Table 9: Summary of the performance of the RF photoinjector.

Parameter	
E_z flatness at cavity peaks	>99%
Resonant frequency, f_π	11993.996 GHz
Mode separation, Δf	27.1 MHz
Coupling factor, β	1.005
Filling time, t_F	112.5 ns
max(E_surf) for 1 MV/m at cathode	0.988 MV/m
BDR (for 400 ns pulse length)	5.59 x 10^{-6} bpp/m
max(ΔT) (for 400 ns pulse length)	31 $^\circ$C
Multipactor power zones	0.035-0.560 MW, 1.20-3.10 MW

5 DC electron injector

The Coherence and Quantum Technology (CQT) group at Eindhoven University of Eindhoven is specialized in the development of low energy, low emittance electron guns. Also transport and manipulation of these low energy electron bunches to an interaction point with limited increase in emittance is part of the expertise of CQT. One of the DC photoguns which has been developed at CQT has become a commercial product because of its excellent beam quality, repetition rate (> kHz) and reliability [50-52] More than 10 of these DC guns have been sold and are used as a workhorse for ultrafast electron diffraction experiments all over the world. In this chapter we investigate the possibility to use this electron gun as an injector for an X-band driven FEL.

5.1 Introduction: DC photogun based injector

The proposed setup and what hereafter is called the injector consists of three main components (Fig 24): a 100 kV DC photogun, a 1.5 GHz velocity buncher optimized for 100 keV electron bunches and a high gradient CLIC X-band accelerator adjusted for 100 keV electron injection. Besides of these main components a couple of solenoids are required to control the radial size of the electron bunches during transport and at the entrance of the velocity buncher and accelerator.

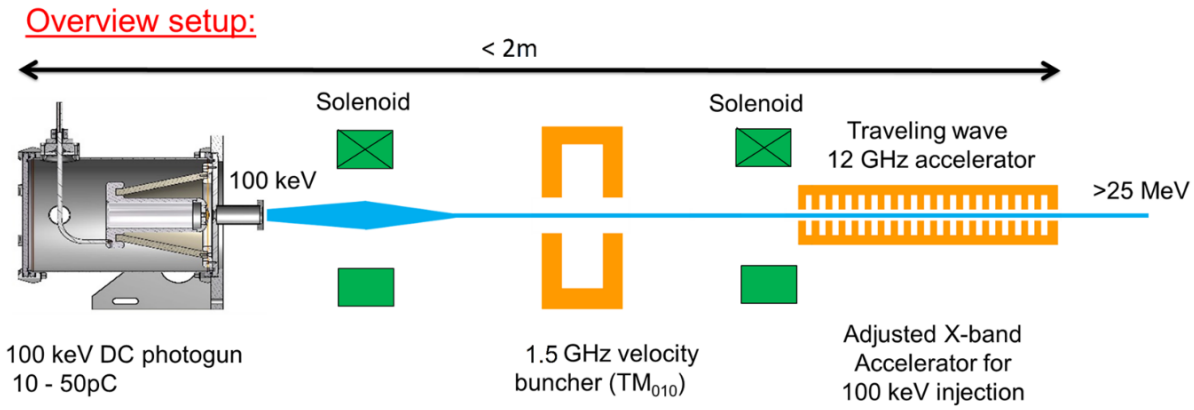

Figure 24: Injector consisting of a 100 keV DC photogun, a 1.5 GHz velocity buncher and an adjusted CLIC X-band accelerator for 100 keV electron injection.

The primary purpose of this injector concept is to investigate the possibility to generate electron bunches with a charge of 10 pC in a 100 keV DC photogun and directly inject these electron bunches into a high gradient X-band accelerator. Moreover, the electron bunches have to be accelerated to a couple of MeV at the exit of this single X-band accelerator while keeping the normalized emittance, energy spread and bunch length acceptable for injection into the X-band Linac of the FEL. During this first stage the electron bunch properties have been optimized by simulations at the exit of an adjusted X-band accelerator. This has been done for 10 pC bunches with an energy of 20 MeV at the exit of an adjusted X-band accelerator. Based on these simulations a velocity buncher and adjusted X-band accelerator has been designed. This velocity buncher and X-band accelerator will be manufactured in the summer of 2019. By

the fall/winter of 2019 the complete beam line as proposed in Fig. 24 will be built at the CQT group. The experimental results will be used to validate the results from the simulations.

The secondary purpose is to investigate by simulations and experiments the possibility to increase the charge from 10 pC to 75 pC. Also additional acceleration to 300 MeV of the 10 and 75 pC bunches will be examined by simulations. The simulations of this extra acceleration will be done by adding a couple of standard CLIC X-band structures to the setup shown in Fig. 24.

5.2 DC photo gun

The electron gun used for the simulations was originally designed at the CQT group and is now commercially available [50-52]. In Fig. 25, on the left, a picture is shown of the DC gun and on the right a 3D cross section of the vacuum vessel of the gun. Inside the vacuum vessel an aluminum conductor at a voltage of -100 kV is supported by a PEEK cone which is connected to the vacuum vessel. The 100 kV high voltage feedthrough is custom made and very compact, connecting the external HV power supply to the aluminum conductor inside the vacuum can. This HV power supply fits into a standard 19” rack.

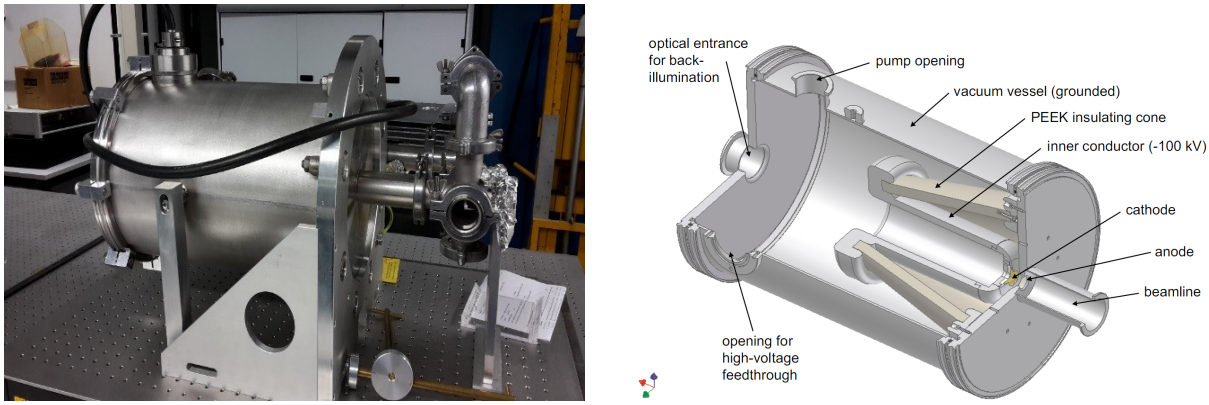

Figure 25: Picture and 3-Dimensional view of the design of the 100 kV DC photogun. Photoemitted electrons are accelerated towards the anode and are entering the beam line via the hole in the anode [1].

A magnification of the cathode-anode section can be seen in Fig. 26. A copper cathode is installed inside the aluminum conductor and can be replaced when damaged. A sub-picosecond UV-laser pulse hits the copper cathode to free an electron bunch from the cathode. The bunch is instantaneously accelerated by the DC electric field between cathode and anode. The cathode is slightly tapered towards the anode and optimized to generate an electric field with maximum field strength of 10 MV/m on the cathode. A solenoid is placed directly at the exit of the DC-gun to counteract space charge forces and thus prevent the bunch from expanding too fast during the initial phase of the acceleration. This is essential to minimize emittance growth during this phase. This gun was originally built to accelerate 100 fC bunches with a normalized transverse emittance of 40 nm [53]. By using 100 times more UV-energy and a UV-spot on the cathode with a 10 times bigger radius an electron bunch of 10 pC can be extracted with the

same charge density at the cathode.

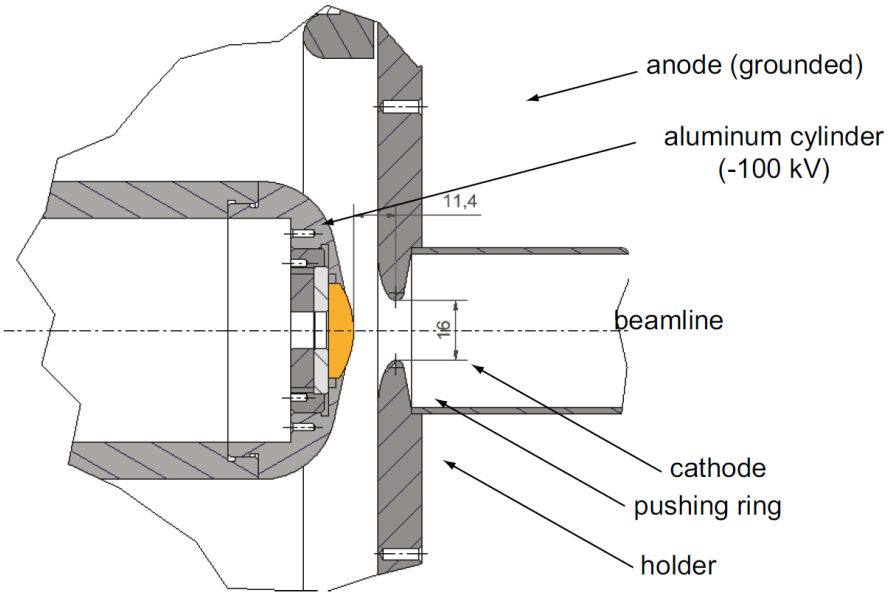

Figure 26: Technical drawing of a bulk copper photocathode clamped in the holder. A ring is pushing at the back to ensure electrical contact between the cathode and the holder [2].

The HV power supply applies a constant 100 kV potential difference between cathode and anode. This implies that the repetition rate of the electron bunches generated by this DC gun can only be limited by either the repetition rate of the UV-laser or the maximum current the HV power supply can provide. The 100 kV power supply can deliver an average current of 1 mA, corresponding to 100 pC bunches at 10 MHz rep rate. The repetition rate of a UV-laser system is typically around 1 kHz but systems up to several MHz are commercially available. In principle the gun could therefore operate at several MHz, so the FEL will be limited by the repetition rate of the klystrons (up to 1 kHz) which drive the RF-accelerator of the FEL Linac.

5.3 Velocity buncher cavity

Due to the low kinetic energy (100 keV) of the electrons at the exit of the photogun space charge effects will have strongly influence the behavior of the electron bunch. Directly after being created at the cathode the electron bunch will undergo a rapid expansion in both the radial direction and the longitudinal direction. The expansion in the radial direction is controlled by the solenoid placed at the exit of the DC photogun. A 10 pC electron bunch generated by a 500 fs UV laser pulse on a 200 μm rms radius spot on the cathode of the photogun will expand to an electron bunch with a length of approximately 50 ps (FWHM) at a distance of 30 cm from the cathode, i.e. an expansion of approximately 150 ps per m distance travelled. Simulation have shown that the duration of a 100 keV electron bunch should not be longer than 5 ps for it to be injected directly into a 12 GHz X-band accelerator. This is necessary to achieve satisfying results at the exit of this X-band accelerator. Therefore, the first cell of the X-band accelerator should be positioned at a distance of 2 cm from the cathode which is impossible form a physical point of view. Another possibility is to compress the electron bunch

back to a length of 5 ps at the entrance of the X-band accelerator by using a velocity buncher RF cavity operating in the TM_{010} mode. A Ω-cavity is being designed and the RF frequency has been maximized. This is done to minimize the cavity size and to minimize the required RF power for the velocity buncher. Furthermore, to enable proper synchronization, the 12 GHz of the X-band accelerator frequency (12 GHz) should be an even harmonic of the RF frequency of the velocity buncher. GPT [54] and CST [55] simulations for a 10 pC electron bunch have shown that the highest possible frequency for the velocity buncher in this setup is 1.5 GHz. Here the center of the velocity buncher is placed at a distance of 30 cm form the cathode and the entrance of the X-band accelerator at a distance of 70 cm from the cathode. The RF design, done with CST Microwave Studio is illustrated in Fig. 27. A rather big bore radius of 1 cm has been chosen to allow free passage and proper compression (without too much emittance growth) of electron bunches with charges over 10 pC.

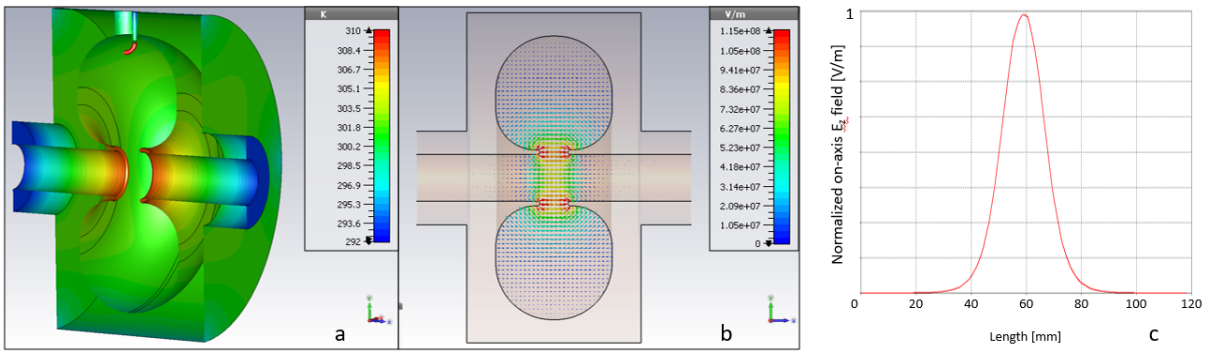

Figure 27: CST simulations of a 1.5 GHz velocity buncher for 100 keV electrons. a) Temperature at 350 W continuous input power. b) Electric field profile at a longitudinal cross section. c) Normalized on-axis E_z- field.

To compress the electron bunches to the required pulse duration at the entrance of the X-band accelerator, while preventing excessive emittance growth, the maximum on-axis RF electric field strength inside the velocity buncher should be approximately 2 MV/m, corresponding to an RF power of 350 W. The required continuous RF power and RF electric field strength can be kept low because electrons at 100 keV are not yet highly relativistic. A small change in kinetic energy of the electron imposed by the velocity buncher will result in a sufficient change in velocity of the electrons to compress the electron bunch back to 5 ps over a relative short distance. Relativistic electrons would require much more change in kinetic energy to be compressed over such a small distance but would result in a high energy spread which is not acceptable. Because of the continuous RF power the velocity buncher is also not limiting the repetition rate of the FEL.

5.4 X-band accelerator design for 100 keV injection

The 100 keV compressed electron bunches now need to be injected directly into an X-band accelerator to be accelerated to relativistic energies. Unfortunately injecting these bunches directly into a CLIC X-band accelerator does not work because the CLIC X-band accelerators were designed for injection of highly relativistic electron bunches. The speed of electrons at 100 keV is only $0.55c$, with c the speed of light. The CLIC accelerators are traveling wave structures which a phase advance of $2\pi/3$. 100 keV electrons injected at the right injection

phase of the CLIC accelerator will not reach the second cell once the phase of the accelerator has changed by $2\pi/3$ but will only be approximately halfway the first cell. At this point the electron will be decelerated and even returned towards the entrance of the accelerator. The first cells of the CLIC X-band accelerator are simply too long to accept injection and acceleration of 100 keV electrons. Therefore, the length of the first 3 cell of a CLIC X-band accelerator have been shortened and optimized for 100 keV electrons injection given an RF input power of 10 MW (Fig 28). The dimensions of the aperture are the same as the CLIC T24 structure but the first 3 cells are shortened respectively by 2.5 mm, 1 mm and 0.5 mm. As a result, the radii of all cells in the structure and the input and output coupler had to be adjusted in HFSS [56]. Because the standard CLIC structure has an RF power transmission of 55% it was decided to lengthen the accelerator to 50 cells instead of the standard 24-26 cells of the standard CLIC accelerator sections. This 50 cell structure has a power transmission of 23%. The repetition rate of this 50 cell accelerator is limited by the klystron repetition rate. The 6MW Scandinova klystron modulator used in the XBOX3 test stand at CERN can go up to a repetition rate of 1 kHz with an output power of 3 MW. After an RF pulse compressor this gives an RF power of around 10 MW. Therefore, the 50 cell accelerator has been optimized for 10 MW input power.

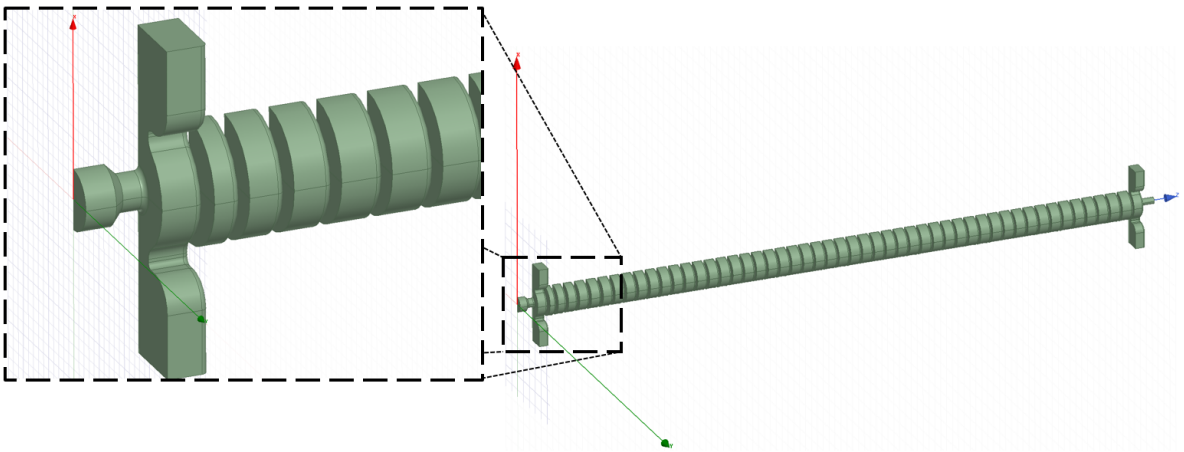

Figure 28: 50 cells X-band accelerator design optimized for 100 keV electron injection (100XS50) based on the standard CLIC X-band accelerator design (T24). The first 3 cells have been shortened.

The complex magnitude of the on-axis electric field in z-direction is plotted in Fig. 29. The field is lower in the first adjusted cells but still sufficient to accelerate injected 100 keV electrons to > 1 MeV in the first 3 cells. At the exit of the 3rd cell the velocity of the electrons is approximately $0.95c$. Ideally also the length of the following up cells should therefore be adjusted, but simulations showed this was not strictly necessary for this 10 pC setup. The first 24 apertures are copied from a T24 structure and are tapered towards the end. To make the apertures not too small after cell 24 - compared to the electron beam size - it has been decided to keep the size of the apertures the same from cell 25 to 50. As a result, this 50 cell accelerator is a combination of a constant gradient (cell 1 till 24) and a constant impedance (cell 25 till 50) accelerator. This is apparent from the behavior of the complex magnitude of the on axis E field (Fig. 29), which increases till cell 24 and then decreases from cell 25 onwards. Even more cells could be added to the 50 cell structure to gain extra energy since still 23% of the RF power is still available. In Fig 30 the imaginary vs the real part of the on-axis electric is

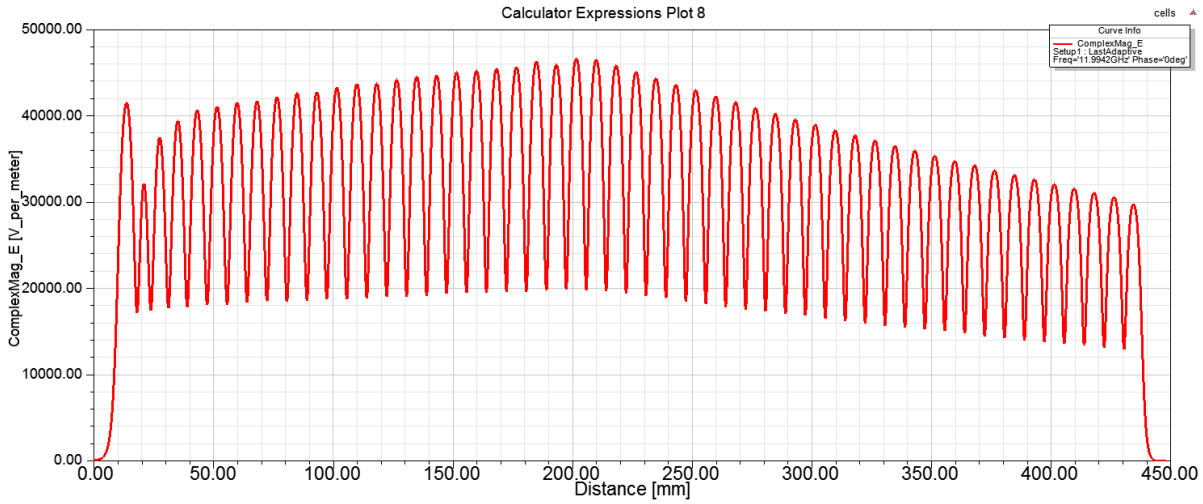

Figure 29: Complex magnitude of the on axis E_z field of the 50 cell accelerator for 100 keV electron injection

shown for a frequency of 11.9942 GHz. It turns out that the 50 cell structure is well tuned with a phase advance of $2\pi/3$.

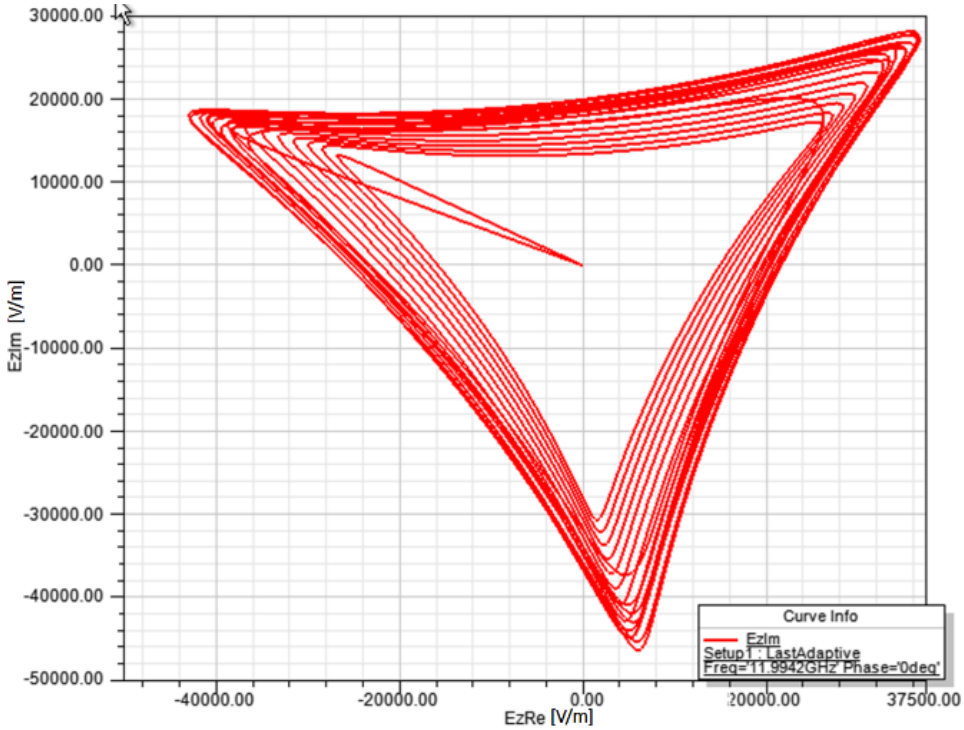

Figure 30: Real versus Imaginary part of the on-axis E_Z field

5.5 Beam dynamics results

GPT simulations of the electron bunches have been done over the complete length of the injector from the cathode surface till the exit of the adjusted X-band accelerator (Fig 24). These simulations included space charge effects and have been done with 10^5 macro particles. The

3D EM field maps (from CST Microwave Studio) of the DC photogun and the velocity buncher have been used in the simulations. Field expansions of the on-axis electric field in z-direction (from HFSS) have been used to calculate the EM fields close the axis. Simulations show that during acceleration no electrons were more than 1 mm off-axis in the 50 cell accelerator. A 1 mm off-axis limit has been cross checked with simulations with the complete 3D EM field maps of the 50 cell accelerator and turned out to be a good approximation. The RF power used to drive the velocity buncher was 350 W and 10 MW for the 50 cell X-band accelerator. The 10 pC electron bunches were created by a 500 fs (FWHM) UV laser pulse. The laser pulse has a Gaussian shape in the radial direction and the temporal direction but is cut off at 2 sigma in the radial direction, resulting in a better electron bunch quality at the exit of the X-band accelerator. The rms transverse size of the laser pulse is 200 μm. This results in a thermal emittance of 0.1 μm for the electron bunch at the cathode surface. The solenoid currents, the RF phases of the velocity buncher and the accelerator and the RF power in the velocity buncher have been optimized to achieve optimal electron bunch properties at the exit of the 50 cell X-band accelerator.

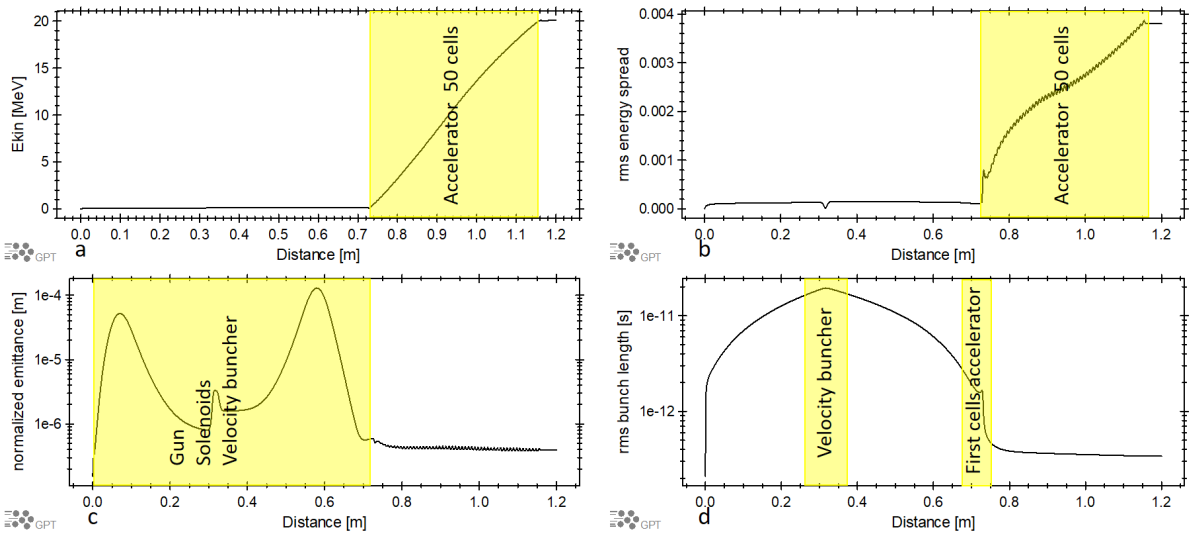

Figure 31: GPT simulations of the electron beam properties along the beamline. Horizontal axis is the distance from the cathode (0m) till the exit of the X-band accelerator (1.2m). a) Kinetic energy, b) rms energy spread, c) normalized emittance and d) rms bunch length.

An overview of several beam parameters along the beam line are shown in Fig. 31. 100 keV electron bunches are injected into the 50 cell accelerator and gain 20 MeV kinetic energy. The acceleration is nearly linear over the entire length of the accelerator. The energy spread however increases from 0.02% to 0.38% inside the accelerator. The energy spread increases faster in the second part of the accelerator, i.e. the constant impedance part. This might indicate that a constant gradient 50 cell accelerator could be beneficial for the energy spread but that would require bigger apertures at the entrance of the accelerator and therefore would result in less energy gain. Bigger apertures however should accommodate for higher charge to be accelerated and is therefore definitely worth investigating. However, this will require a very time-consuming new RF design of the accelerator. The normalized emittance grows from 0.1 μm rad at the cathode to only 0.4 μm rad at the exit of the X-band accelerator. During ac-

celeration in the DC gun the electron bunch expands from 200 fs (rms) at the cathode to 2 ps at the exit of the DC gun over a distance of only 2 cm. Between the exit of the DC gun and the center of the velocity buncher, which is placed at 20 cm from the cathode, the electron bunch expands to 20 ps rms. The electron bunch is compressed back to 2 ps at the entrance of the adjusted X-band accelerator is compressed even further to ∼500 fs in the first few cells of the accelerator. At the exit of the accelerator the electron bunch length is 350 fs. An overview of the electron bunch parameters at the exit of the DC gun and at the exit of the adjusted X-band accelerator can be found in table 10.

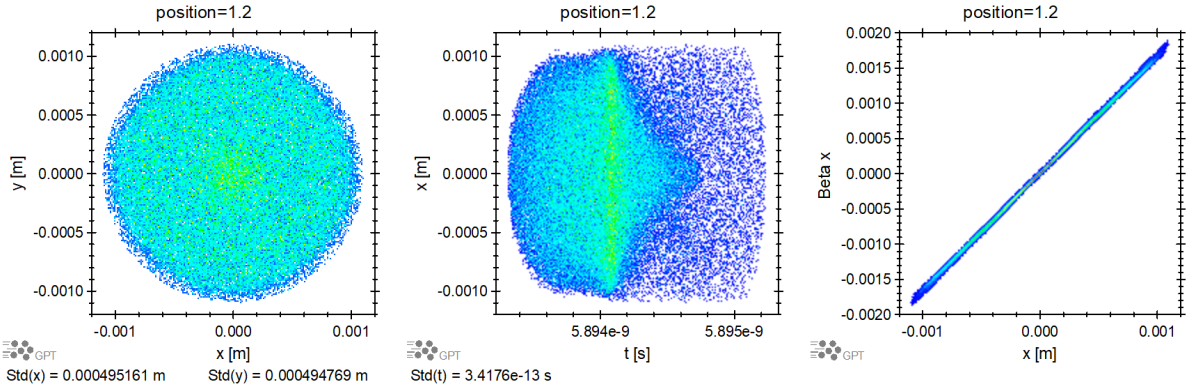

Figure 32: GPT simulations with 100.000 macro particles of the profile of the electron bunch at the exit of the accelerator. a) front view of the bunch (y vs x), b) side view of the bunch (x vs t), and c) phase space in x direction (β_x vs x).

The bunch profile at the exit the adjusted X-band accelerator (1.2 m from the cathode) is shown in Fig 32. The x-y distribution is cylindrically symmetric with an rms size in the radial direction of 0.5 mm. All electrons are within 1 mm distance from the axis. The side view of the bunch (x-t distribution) shows a higher density towards the front of the electron beam. This indicates that the phase of velocity buncher and accelerator are not completely optimized and the electron bunch can be compressed below 350 fs. In Fig 32c. the phase space distribution in the x-direction is plotted, showing a linearly expanding bunch. The bunch behavior in the y-direction is similar.

Table 10: Electron bunch properties at the exit of the DC-photogun and the adjusted X-band accelerator.

	e- bunch at exit DC photogun	e- bunch at exit adjusted X-band accelerator
Charge	10 pC	10 pC
Kinetic energy	100 keV	20 MeV
rms energy spread	0.01 %	0.38 %
rms bunch length	2 ps	350 fs
Normalized emittance [Hz]	0.1 μm	0.4 μm

5.6 Experimental results

The simulations done for the 10 pC case and RF designs of the velocity buncher and the 50 cell accelerator - as described in the previous sections - will be tested by experiments is the fall/winter of 2019 at the CQT group. At this moment (May 2019) the technical drawings (Fig. 33a) of the 50 cell accelerator are finished and the accelerator disks are being made by the company VDL. Also a 12 GHz RF pulse compressor is being made and a 6 MW Scandinova klystron/modulator has been ordered. The design of the 1.5 GHz velocity buncher is almost finished. It is expected that all parts (Fig 33b) for the injector setup will be ready by the fall of 2019.

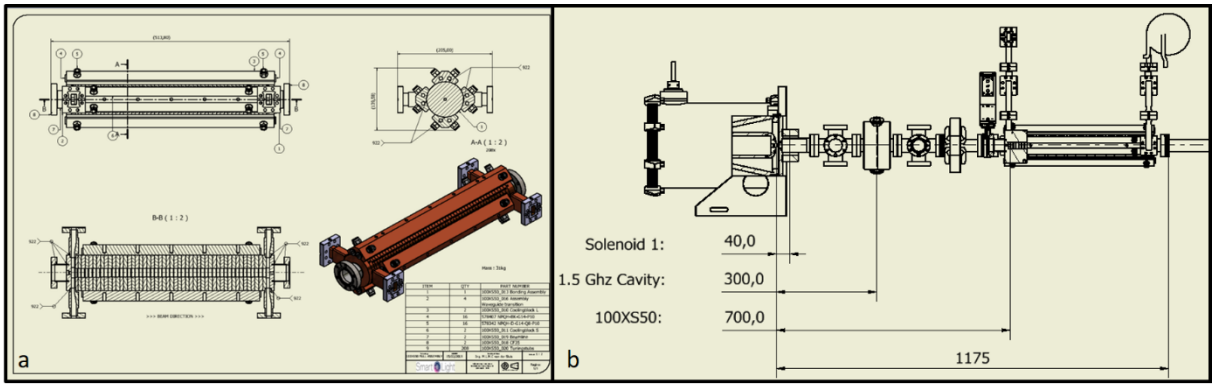

Figure 33: Technical drawing of the 50 cell X-band accelerator for 100 keV injection (a) and the experimental beamline (b).

5.7 Conclusions and outlook

Simulations have shown that an injector consisting of a 100 keV DC photogun in combination with a 1.5 GHz velocity buncher and an adjusted CLIC X-band accelerator can produce 10 pC electron bunches with a kinetic energy of 20 MeV, an energy spread of 0.4%, an emittance of 0.4 μm and an rms pulse length of 350 fs. The repetition rate of the DC photogun can be in the MHz range but the injector is limited by the repetition rate of the X-band klystron (1 kHz) which drives the adjusted X-band accelerator. This system will be built by the fall off 2019 to confirm the results from the simulations. Investigation of increasing the charge to 75 pC still need to be done and is most probably feasible. This might already be possible in the first setup to be built. If necessary, the following upgrades can be studied to achieve 75 pC bunches with the desired properties for injecting into the FEL Linac:

1. DC-photogun operating at 200 keV to extract more charge with less space charge effects.

2. A velocity buncher with a lower frequency to achieve a better compression at high charge.

3. A redesign and further optimization and fine-tuning of the adjusted X-band accelerator. More cells at the entrance could be shortened and the aperture should be made bigger to allow for more charge to pass at low kinetic energy.

None of these adjustments will affect the repetition rate.

6 Considerations about Laser and Photocathode systems

In the radiofrequency (RF) photo-injectors the electrons are produced via the photoelectric effect by a suitable laser impinging on a photocathode mounted inside an RF gun. The photocathode material in an RF photo-injector is of vital importance since it determines the intrinsic emittance and the quantum efficiency (QE) of the electron source.

The semiconductor materials like Cesium Telluride (Cs_2Te) provide a QE, which are orders of magnitude larger than metal photocathodes like copper (Cu) or Magnesium (Mg); while the expected intrinsic emittance for both types of material is similar.

The selection criteria applied for our Compact Light project to define the proper photocathode and the relative laser device for the cathode illumination. The main criteria are related with the high quantum efficiency, high robustness and fast response time in addition with low intrinsic emittance, low surface roughness and low lifetime.

Intrinsic emittance measurements with the same injector have been obtained by changing the photocathode Cu vs Cs_2Te, at SWISS FEL Injector Test Facility [57]. Similar ASTRA simulations have been obtained by our collaboration for the two photocathodes, showing that the difference in intrinsic emittance for the two types of material is not significant in view of accelerator applications.

The specifications [58] of the beam in our project, in the table 1 are guiding to the laser and the photocathode selection, in addition with the fundamental condition of the 100 MV potential applied in the RF-gun:

A copper photo-cathode is proposed as the base-line electron source candidate for our case, as it is also fulfilling the SwissFEL injector requirements [59] in terms of beam brightness. For the operation, a laser system capable of generating up to 200 pC of photo-electrons is required corresponding to a minimum energy per pulse of 100 μJ at 266 nm on the Copper surface, assuming a QE of 10^{-5}. Such pulse energies can be achieved by a Ti:Sapphire laser system providing short pulses of 50 fs, generating a uniform longitudinal profile with a rise time of a few 100 fs. The Ti:Sapphire provides broad, continuous tuning range from 700-1000 nm using a single optics set with custom wavelength ranges available <700 nm or >1000 nm ultra-narrow linewidths from <50 kHz absolute linewidth, with options to achieve Hertz level linewidth via an external, ultra-stable reference. Similar wavelengths at 262 nm can be obtained by the 4th harmonic of the Nd:YLF (Yttrium Lithium-Fluoride) [60] or the Yb:Ca_2F lasers [7].

It can, also, be proposed an acetone Laser-Induced-Fluorescence (LIF) laser [61, 62], providing wavelengths 466 nm and 282 nm or an optical frequency standard based on laser-cooled and trapped ^{199}Hg* ions providing wavelengths at 194 nm and 282 nm [63]. In addition, many diagnostic tools and pulse-shaping techniques are available for the near-IR / visible spectral region, and frequency tripling of the fundamental laser wavelength allows easy access to the UV region. In order to produce a homogeneous flat-top electron beam profile (transversally) on the cathode surface, the laser intensity profile must also be flat-top.

Another promising option are the Yttrium photocathodes, a silvery-metallic transition metal

[64,65] that provides a good compromise of high quantum efficiency, low emittance and robustness. Differently from the Cu work function ($\varphi_{work} \sim$ 4.6 eV), yttrium has a work function of about φ_{work} = 3 eV. This value is very interesting because it gives, in principle, the possibility to illuminating the photo-cathode with an incidence radiation in the visible range at $\lambda \sim$ 400 nm. This wavelength can be obtained as second harmonic of Ti:Sa laser, and for this it is possible to generate the linear electron photoemission with metals by means of visible radiation instead of UV radiation. This opportunity avoids the use of higher harmonic conversions and, giving an increase of the laser energy per pulse, allows the realization of high repetition rate photoinjector by using conventional laser sources. First intrinsic emittance and quantum efficiency studies of yttrium thin film on Cu photo-cathodes have been performed in a RF photoinjector [65,66] using the UV radiation.
From the theoretical calculation the theoretical intrinsic emittance is $\varepsilon_{yttrium}$ = 1.1mmmrad/mm at E_{peakRF} = 110 MV/m using λ = 266 nm and QE $\sim$ 5.4 x 10^{-4}. Using λ = 400 nm, the theoretical intrinsic emittance is $\varepsilon_{yttrium}$ = 0.43 mmmrad/mm at E_{peakRF} = 110 MV/m and QE $\sim 10^{-5}$. The QE value with λ = 400nm is similar to the copper value.

The laser selection is a relatively easy problem to be fix in relation with the photocathode to be selected among the Ti:Sapphire, Nd:YAG (2^{nd} harmonic) or Nd:YAF (4^{th} harmonic). On the other side, even if the weak point of the photocathode Cu is the low Q.E. of the order of 10^{-4} - 10^{-5} at about 6.3 eV photon energy equal to 196.3 nm; it has many important characteristics like the long life-time, i.e. order of years, very small dark current and operates in high accelerating gradient. The last property is one of the basic specification for our case. The Cs_2Te photocathode is also implemented for low voltage RF-cavity with excellent results; taking into account the high Q.E. in UV light and its reliability but the very small life-time, i.e. $\sim$ <50h> and very sensitive to contaminations.

7 References

1. M. Xie, ”Design Optimization for an X-ray FEL driven by SLAC linac”, Proc. of PAC Conference, 1995.
2. E. A. Seddon et al., ”Short-wavelength free-electron laser sources and science: a review”, Reports on Progress in Physics, Volume 80, Number 1.
3. B. E. Carlsten, Nucl. Instrum. Methods A 285, 313 (1989).
4. L. Serafini, J. B. Rosenzweig, Phys. Rev. E 55 (1997) 7565.
5. J. B. Rosenzweig and E. Colby, ”Charge and Wavelength Scaling of RF Photoinjector Designs”, in Proc. of Advanced Accelerator Concepts, AIP Conf. Proc. 335 724 (1995)
6. M. Boscolo et al., ”Single spike operation in SPARC SASE-FE”, Nucl. Inst. And Meth. A, Volume 593, Issues 1-2, 1 August 2008, Pages 137-142.
7. T. Shintake et al., ”A compact free-electron laser for generating coherent radiation in the extreme ultraviolet region”, Nature Photonics, vol. 2, Sept. 2008
8. D.T. Palmer et al., SPIE 2522 (1995) 514.
9. P.R. Bolton, et al., SLAC-PUB-8962 LCLS-TN-01-05 Revised November 2001.
10. R. Akre, et al., SLAC-PUB-13014 November 2007.
11. C. Limborg-Deprey, et al., LCLSTN- 05-3, Feb. 2005.
12. L. Xiao, et al., PAC2005, Knoxville, TN, pp. 3432-3434 (2005).
13. D.H. Dowell et al., PAC 2007, Albuquerque, NM, pp. 1296-1298 (2007).
14. D. Alesini, et al., PRAB 18, 092001 (2015)
15. D. Alesini, et al., PRAB 21 112001 (2018).
16. D. Alesini, et al., IPAC2017
17. D. Alesini et al., Process for manufacturing a vacuum and radio-frequency metal gasket and structure incorporating it, International Patent Publication No. WO 2016/147118 A1, assigned to INFN.
18. Militsyn, et al., LINAC2016.
19. J.W. McKenzie et al., IPAC’14, Dresden, Germany, June 2014, pp. 2983-2985.
20. J.W. McKenzie et al., IPAC’14, Dresden, Germany, June 2014, pp. 2983-2985.
21. L. Cowie et al., 28th Int. Linear Accelerator Conf., East Lansing, MI,USA, September 2016.
22. R. Zennaro et al., Proceedings of LINAC2014, p. 333, 2014.

23. M. Ferrario et al. Experimental demonstration of emittance compensation with velocity bunching. Physical review letters, 104(5):054801, 2010.

24. A. Grudiev, S. Calatroni, W. Wuensch, ”New local field quantity describing the high gradient limit of accelerating structures”, Physical Review Special Topics Accelerators and Beams, 12, 102001 (2009).

25. V. A. Dolgashev, PAC 2003, p. 1267.

26. W. Wuensch, in Proceedings of the International Particle Accelerator Conference, IPAC 17, 2017.

27. C. Limborg et al., Report No. LCLS-TN-05-3,

28. D. Alesini et al., gun eli PRAB 21, 112001 (2018)

29. C. Nantista et al., Low-field accelerator structure couplers and designtechniques, Phys. Rerv. ST Accel. Beams7(2004) 072001

30. https://www.cmlengineering.com/

31. R. Zennaro, et al., IPAC2013, p. 2827.

32. http://www.pulsar.nl/gpt/. General Particle Tracer.

33. J. Arthur, et al. Linac coherent light source (LCLS) conceptual design report. No. SLAC-0593. 2002.

34. B.E. Carlsten, "New photoelectric injector design for the Los Alamos National Laboratory XUV FEL accelerator. Nuclear Instruments and Methods in Physics Research Section A: Accelerators, Spectrometers, Detectors and Associated Equipment 285.1-2 (1989): 313-319.

35. M. Ferrario et al. "HOMDYN study for the LCLS RF photo-injector."The Physics of High Brightness Beams. 2000. 534-563.

36. M. Ferrario et al. Direct measurement of the double emittance minimum in the beam dynamics of the sparc high-brightness photoinjector. Physical review letters, 99(23):234801, 2007.

37. D. H. Dowell and J. F. Schmerge. Quantum efficiency and thermal emittance of metal photocathodes. Physical Review Special Topics-Accelerators and Beams, 12(7):074201, 2009.

38. W. S. Graves et al. ”Measurement of thermal emittance for a copper photocathode.” PACS2001. Proceedings of the 2001 Particle Accelerator Conference (Cat. No. 01CH37268). Vol. 3. IEEE, 2001.

39. M. Ferrario et al. Experimental demonstration of emittance compensation with velocity bunching. Physical review letters, 104(5):054801, 2010.

40. K. Halbach and R. F. Holsiger, ”SUPERFISH - A Computer Program for Evaluation of RF Cavities with Cylindrical Symmetry”, Particle Accelerators, Vol. 7, pp. 213-222, 1976.

41. A.E. Vlieks, V. Dolgashev, S. Tantawi, S. Anderson, F. Hartemann, Roark Marsh, ”X-band RF gun development”, pp. 3816-3818, Proceedings of IPAC’10, Kyoto, Japan

42. A. Aksoy, RF gun design, private communication, unpublished.

43. E. Somersalo, P. Ylä-Oijala, D. Proch, and J. Sarvas, ”Computational methods for analyzing electron multipacting in RF structures”, Particle Accelerators, vol. 59, pp. 107-141, Aug. 1998.

44. R. Vaughan, ”Secondary emission formulas”, IEEE Transactions on Electron Devices, Vol. 40, no. 4, pp. 830-839, Apr. 1993.

45. D. González-Iglesias, A. M. Pérez, S. Anza, J. Vague, B. Gimeno, V. E. Boria, D. Raboso, C. Vicente, J. Gil, F. Caspers, L. Conde, ”Multipactor Mitigation in Coaxial Lines by Means of Permanent Magnets”, IEEE Transactions on Electron Devices, vol. 61, no. 12, pp. 4224-4231, Dec. 2014.

46. B. G. Martinez et al., to be published

47. D. P. Pritzkau, ”RF Pulsed Heating”, SLAC-Report-577, Ph.D. Dissertation, Stanford University, 2001.

48. A. Aksoy, private communication, unpublished.

49. M. Behtouei, ”Design and Measurements of the High Gradient Accelerating Structures”, PhD Thesis, UniversitÃ di Roma ”La Sapienza”, 2018

50. T. van Oudheusden et al., Electron source concept for single-shot sub-100 fs electron diffraction in the 100 keV range", J. Appl. Phys. 102, 093501 (2007).

51. T. van Oudheusden, Electron source for sub-relativistic single-shot femtosecond diffraction", PhD thesis (Eindhoven University of Technology, 2010).

52. Photogun system, dr.XWorks, URL: https://www.drx-works.nl

53. P. Pasmans, ”Ultrafast electron diffraction: An investigation of fundamental limits”, PhD thesis (Eindhoven University of Technology, 2014).

54. The General Particle Tracer (GPT) code, Pulsar Physics, URL: http://www.pulsar.nl

55. CST microwave studio, Computer Simulation Technology (CST), URL: https://www.cst.com/

56. HFSS: High-Frequency Structure Simulator, Ansys, https://www.ansys.com/Products/Electronics/ANSY
HFSS

57. E. Prat, S. Bettoni, H-H. Braun, R. Ganter, and T. Schietinger Phys. Rev. Accel. Beams 18, 043401 (2015)

58. Compact Light project, EU H020 Research and Innovation Program, Grant Agreement No. 777431, 2018-2020

59. Swiss-FEL Conceptual Design Report, PSI Bericht Nr. 10-04, April 2012

60. G. P. A. Malcolm and A. I. Ferguson, Self-mode locking of a diode-pumped Nd:YLF laser , Optics Letters Vol. 16, No 24, 1967-1969, (1991)

61. L. S. Yuen, J. E. Peters and R. P. Lucht, Pressure dependence of laser-induced fluorescence from acetone, Applied Optics, Vol. 36, No 15, 3271-3277, (1997)

62. R. A. Bryant, J. M. Donbar, J. F. Driscoll, Acetone laser induced fluorescence for low pressure/low temperature flow visualization, Experiments in Fluids 28 (2000) 471-476, Springer-Verlag 2000

63. F.C. Cruz, M. Raumer, J.H. Marqquardt, L. Hollberg and J.C. Berquist, An all solid-state Hg* optical frequency standard, Proc. On 5th Symp. on Frequency Standards and Metrology, 511-513, 1995

64. A. Lorusso, L. Cultrera, V. Fasano, A. Perrone, Detailed studies of photocath- odes based on y thin films grown by pld technique, Nuclear Instruments and Methods in Physics Research Section B: Beam Interactions with Materials and Atoms 269 (24) (2011) 3091-3093.

65. A. Lorusso, M. Trovò, A. Demidovich, P. Cinquegrana, F. Gontad, E. Broitman, E. Chiadroni, A. Perrone, Pulsed laser deposition of yttrium photocathode suitable for use in radio-frequency guns, Applied Physics A 123 (12) (2017) 779.

66. Jessica Scifo, PhD thesis in Accelerator Physics, The characterization of metal photocathode for high brightness electron beam photoinjectors, XXX cycle, University of Rome, La Sapienza